SECRET

DST-2660P-107-81-SPR-7

DEFENSE
INTELLIGENCE
AGENCY

Trends and Developments

Special Issue Detection of Nuclear Materials from Space (U)

20 JULY 1981

NOFORN

SECRET

SPECIAL ISSUE

TRENDS AND DEVELOPMENTS

IN

FOREIGN TECHNOLOGY, WEAPONS AND SYSTEMS

DETECTION OF NUCLEAR MATERIALS FROM SPACE ~~(U)~~

FOREWORD:

~~(S/NOFORN)~~ The application of nuclear reactor electric power supplies to satellite systems by the Soviets had been theorized for the Radar Ocean Reconnaissance Satellite (RORSAT) and many possible means of verification had been discussed. The present paper is an analysis of data obtained through operating on-board gamma radiation detection sensors during chance passages of the U.S. satellites HEAO-1 and HEAO-3 near to the RORSAT COSMOS 954.

(b)(6)

~~(U)~~ This analysis was performed by [redacted] of the Space Sciences Laboratory, The Aerospace Corporation. It was sponsored by Air Force Systems Command/Hq, contract F 04701-80-C-0081 with particular support provided by funds from Air Force Technical Applications Center, PA 8504 and the Mission Oriented Investigation and Experimental Element. Questions or comments should be addressed to [redacted]

(b)(3):10 USC 424

FOR THE DIRECTOR:

(b)(6) [redacted]

TABLE OF CONTENTS ~~(U)~~

DETECTION OF NUCLEAR MATERIALS FROM SPACE (U)

I. SUMMARY AND CONCLUSIONS

(S) Gamma ray data from the A-4 experiment flown aboard the NASA satellite HEAO-1 have provided valuable evidence for the existence of a nuclear reactor aboard COSMOS 954. The investigation described herein obtained this evidence at very low cost by using data from chance encounters between the already orbiting NASA satellite and the Soviet vehicle. COSMOS 954 was detected with 5 significance on December 26, 1977 and with 7 significance on January 11, 1978. The unique signature of each encounter unquestionably establishes the identity of the source for these two events. The spectrum of the detected gamma rays was well fitted to the expected spectrum coming from a reactor. Furthermore the source was readily detectable at a distance of 360 km. Preliminary calculations predicted that a 40 kW reactor would be detectable at 390 km. Thus, the detected gamma rays confirmed the existence of a reactor aboard the RORSAT.

(S) The results of the HEAO-3 RORSAT observations may be summarized as follows:

(1) The RORSAT was detected in the spectrometer shield crystals several times during approaches within 200 km. The observed energy spectrum of the gamma rays is hard, as expected for a reactor, and the direction of the gamma ray source and its time dependence are appropriate for the known position and motion of the RORSAT.

(2) A strong signal was seen in the charged particle detector. If due to reactor neutrons the flux is substantially greater than estimated, cf. Table A1.

(3) When cold and functioning, the germanium detectors (which require cryogenic conditions) were never pointing toward RORSAT. As a result, no gamma spectra were acquired from these sensors.

(8) This study has demonstrated that by using technology more than a decade old the presence of nuclear reactors aboard Soviet RORSAT space vehicles is readily detectable at a range of hundreds of km.

II. Introduction (U)

(S) For some time the Soviet Radar Ocean Reconnaissance Satellites (hereafter, RORSATs) have been presumed to be powered by nuclear reactors. The history of the RORSAT program is given in Table 1. Personnel of the Aerospace Corporation Space Sciences Laboratory considered means of detection of gamma rays from the reactor. The expected gamma ray fluxes were calculated, see Appendix A, and the calculations were independently verified by personnel of the Los Alamos National Laboratory. Techniques using a satellite-borne infrared instrument, a Space Test Program satellite payload, and sounding rocket flights were considered. All of these techniques would have been expensive and the use of a sounding rocket was judged provocative.

(S) A much less expensive approach would be to utilize chance encounters between the RORSATs and satellite-borne gamma ray detection equipment. Two NASA satellites, HEAO-1 and HEAO-3, carried sophisticated astronomical gamma ray sensors. Both had opportunities to detect Soviet RORSATs; see Table 2. The positive detection of gamma radiation from RORSAT reactors by gamma instrumentation carried on these satellites is the subject of this report. Most of the report will deal with the HEAO-1 results since the HEAO-3 data has just become available. The NASA satellite HEAO-1 carries a sophisticated array of low to medium energy gamma ray detectors provided by Professors Laurence E. Peterson of the University of California at San Diego and Walter Lewin of MIT. These HEAO A-4 detectors have much more area than previously has been available, and the HEAO orbit allows it occasionally to pass within 200 km of the RORSATs. HEAO-1 (Vehicle 10217) was launched on August 12, 1977, and approximately one month later the Soviet Union launched two RORSATs, COSMOS 952 and

Table 1
History and Background (U)

YEAR	
1971	FIRST OPERATIONAL FLIGHT OF RORSAT
1972-1977	SEVERAL ANALYTICAL EFFORTS TO DETERMINE CAPABILITY TO DETECT RORSAT USING EXISTING SYSTEMS
1977	LAUNCH OF HEAO-1
1977-1978	ANALYSIS OF HEAO-1/ RORSAT ENCOUNTERS

~~SECRET~~

Table 2
Satellite Parameters

NAME	LAUNCH DATE	INCLINATION (deg)	ALTITUDE RANGE (km)
HEAO 1	12 AUG 1977	23	424-444
COSMOS 952	16 SEP 1977	65	250-260
COSMOS 954	18 SEP 1977	65	251-264
HEAO 3	20 SEP 1979	44	457-478
COSMOS 1176	29 APR 1980	65	248-261

~~SECRET~~

COSMOS 954 (Vehicles 10358 and 10361). Table 2 list the parameters of the three satellites. The RORSATs were always lower than HEAO-1, and occasionally they passed nearly directly below the satellite at a distance as small as 180 km. Table 3 compares the HEAO-1 experiments with other satellite-borne gamma ray detectors in terms of ability to detect nuclear material aboard a RORSAT. The last column gives a figure of merit, the detector volume divided by the distance of closest approach between RORSAT and detector. HEAO-1 is seen to be superior to all other detectors by 2-3 orders of magnitude. At the time Table 3 was prepared HEAO-3 had not been launched. The HEAO-3 detector is roughly comparable to the HEAO-1 in sensitivity. Estimates indicated that the HEAO-1 detectors could detect the gamma rays from a 40 kW reactor at a distance of 390 km with 3σ confidence. Since the HEAO field of view is at most 43^{0} and is scanned by rotation of the satellite about the satellite-sun line, we estimated that in about 10% of such close encounters HEAO A-4 would be pointed properly and could detect the gamma rays.

(8) Using ADCOM orbit elements we calculated all encounters between COSMOS 952 and COSMOS 954 with a range less than 500 km. One hundred twelve such encounters were found: 14 during the 2 1/2 week useful lifetime of COSMOS 952, and 98 for the four months between the launch and reentry of COSMOS 954. Dr. James Matteson, a member of Dr. Peterson's research group, provided us with HEAO A-4 data at times of our choosing. The effort was concentrated on 23 encounters for which the minimum range was less than 200 km. For two HEAO-1 encounters or "events" the RORSAT gamma rays were detected with greater than 5 certainty. The next section of this report is an account of the detection technique used and of the analysis of the positive detection "events" that were found.

Table 3
Spacecraft Gamma Ray Detectors (U)

SATELLITE	DETECTOR TYPE	DETECTOR VOLUME, V	DISTANCE OF CLOSEST APPROACH, R*	FIGURE OF MERIT V/R^2 (cm^3/km^2)
DMSP				
SENSOR 1	CsI	35.4 cm^3	575 km	1.0×10^{-4}
SENSOR 2	CsI	50.5 cm^3	575 km	1.5×10^{-4}
DSP				
SENSOR 1	CsI	5.5 cm^3	35,000 km	4.4×10^{-9}
SENSOR 2	CsI	43.2 cm^3	35,000 km	3.4×10^{-8}
VELA	CsI	10.0 cm^3	120,000 km	7.0×10^{-10}
HEAO-1	PHOSWICH (NaI/CsI)	1300.0 cm^3	180 km	4.0×10^{-2}

*Source at 260 km altitude

~~CONFIDENTIAL~~

III. HEAO-1 MEASUREMENTS (U)

A. DETECTION (U)

(U) A number of factors must be considered in establishing the positive detection of a gamma ray source. The first is the geometry, the direction of the source as compared to the detector look direction and the range of the source from the detector. Second, the detector properties such as energy range, field of view, and sensitivity must be considered. Finally, the signature of the event and of possible background detections can be used to establish the identity of the source.

(S) Figure 1 depicts the HEAO-1 satellite, showing the location of the A-4 detectors. In the figure the solar panels are behind the satellite. HEAO-1 rotated about an axis perpendicular to these panels and oriented toward the sun, with a period of about 30 minutes. Thus the A-4 detectors swept out a great circle on the sky, and in certain phases of the orbit the circle crossed the earth beneath the satellite. It was at these times that the RORSAT gamma rays might have been detectable.

(S) The encounter geometry is shown in Figure 2. For a close encounter to occur each vehicle must have been in the appropriate phase of its orbit. Since the satellites had different altitudes and different orbital periods, encounters did not recur on successive orbits but were more widely spaced in time. The figure helps one to understand the unique signature of a RORSAT detection event. First, knowledge of the oribital elements allows the time at which the event occurred to be calculated accurately. Second, the duration of the event can be predicted from the relative motion of the satellites. Because the target was moving, the event is of shorter duration than the detection of a distant fixed clestial source, but event durations did vary.

HEAO-A EXPERIMENTS

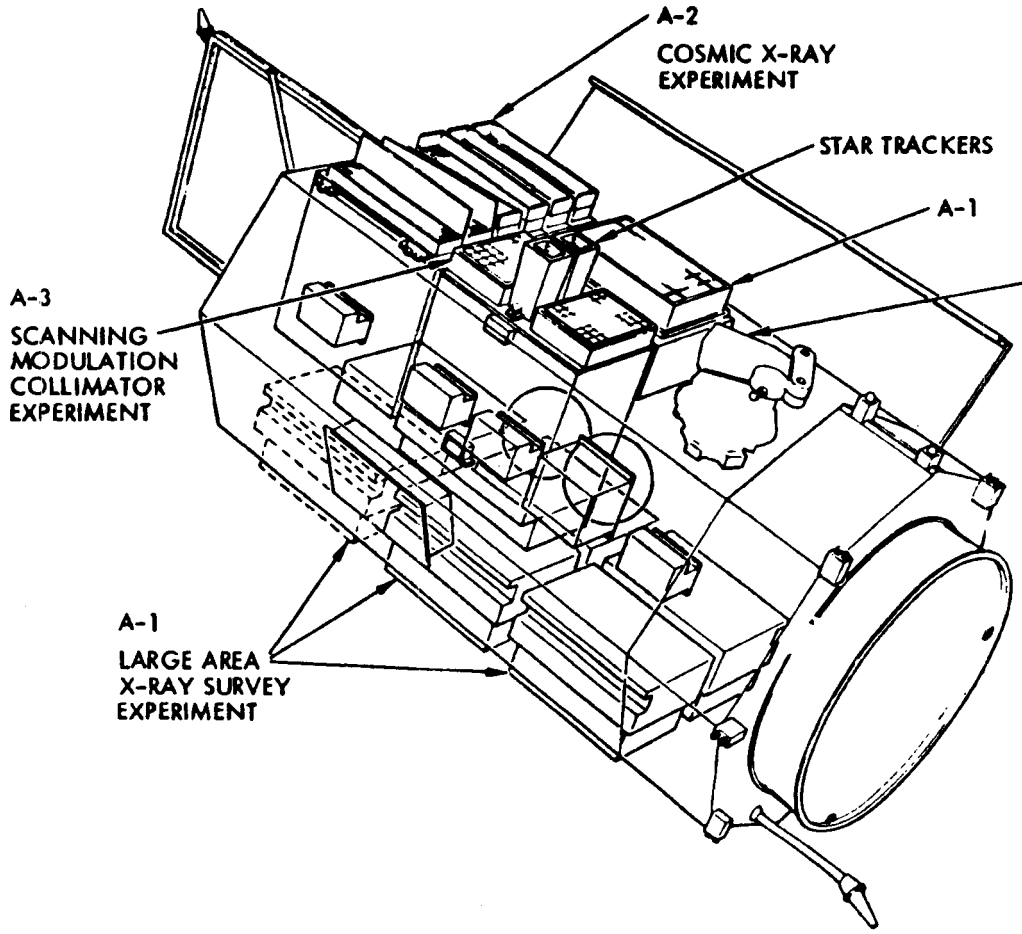

~~UNCLASSIFIED~~

Figure 1

Schematic of Encounter Geometry

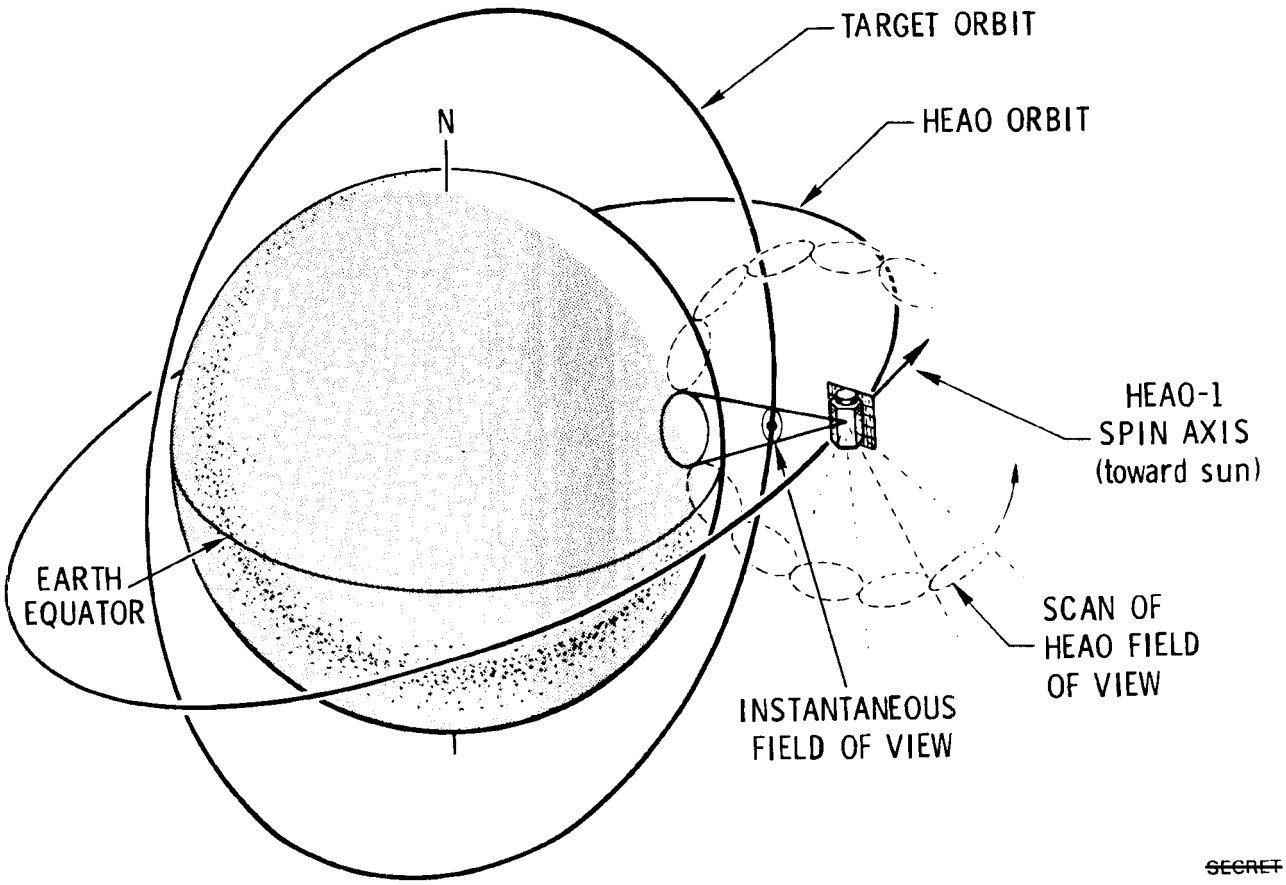

Figure 2

This is illustrated in Figure 3 which shows the motion of COSMOS 954 (361) and HEAO-1 (217) for two encounters. The RORSAT was not detected in either of these encounters because the HEAO A-4 attitude was not appropriate. The HEAO-1 attitude is the third signature criterion; in general HEAO A-4 needs to be looking earthward for detection to occur. Finally, the spectrum of gamma rays from a nuclear reactor can be predicted and therefore constitutes part of the event signature. In summary the unambiguous signature of a RORSAT detection event consists of event timing and duration, HEAO A-4 attitude, and the observed gamma ray spectrum.

~~(U)~~ The UCSD HEAO-1 experiment consists of seven separate actively collimated X-ray and gamma ray detectors. Together the detectors cover the energy range 0.01 - 10.0 MeV. The instrument is shown in Figure 4, and the detector properties are summarized in Table 4. The main detectors are all scintillation counters consisting of thallium-doped sodium iodide crystals (NaI(T1)) viewed by photomultiplier tubes (PMT). Between each NaI(T1) crystal and its PMT is a sodium doped cesium iodide crystal (CsI(Na)) which makes up part of the active shielding. Together the two crystals from a "phoswich". Signals from the CsI(Na) are placed in anticoincidence with NaI(T1) crystals so that NaI(T1) events accompanied by CsI(Na) events can be rejected. This procedure eliminates events in which only part of a photon's energy is left in the main detector. The signals from the two crystals are distinguishable by their different scintillation decay times. In addition to that provided by the phoswich arrangement, active shielding is also provided by eight pieces of CsI(Na) that surround the NaI(T1) scintillators on the sides and define the forward opening apertures. These can be seen in Figure 4.

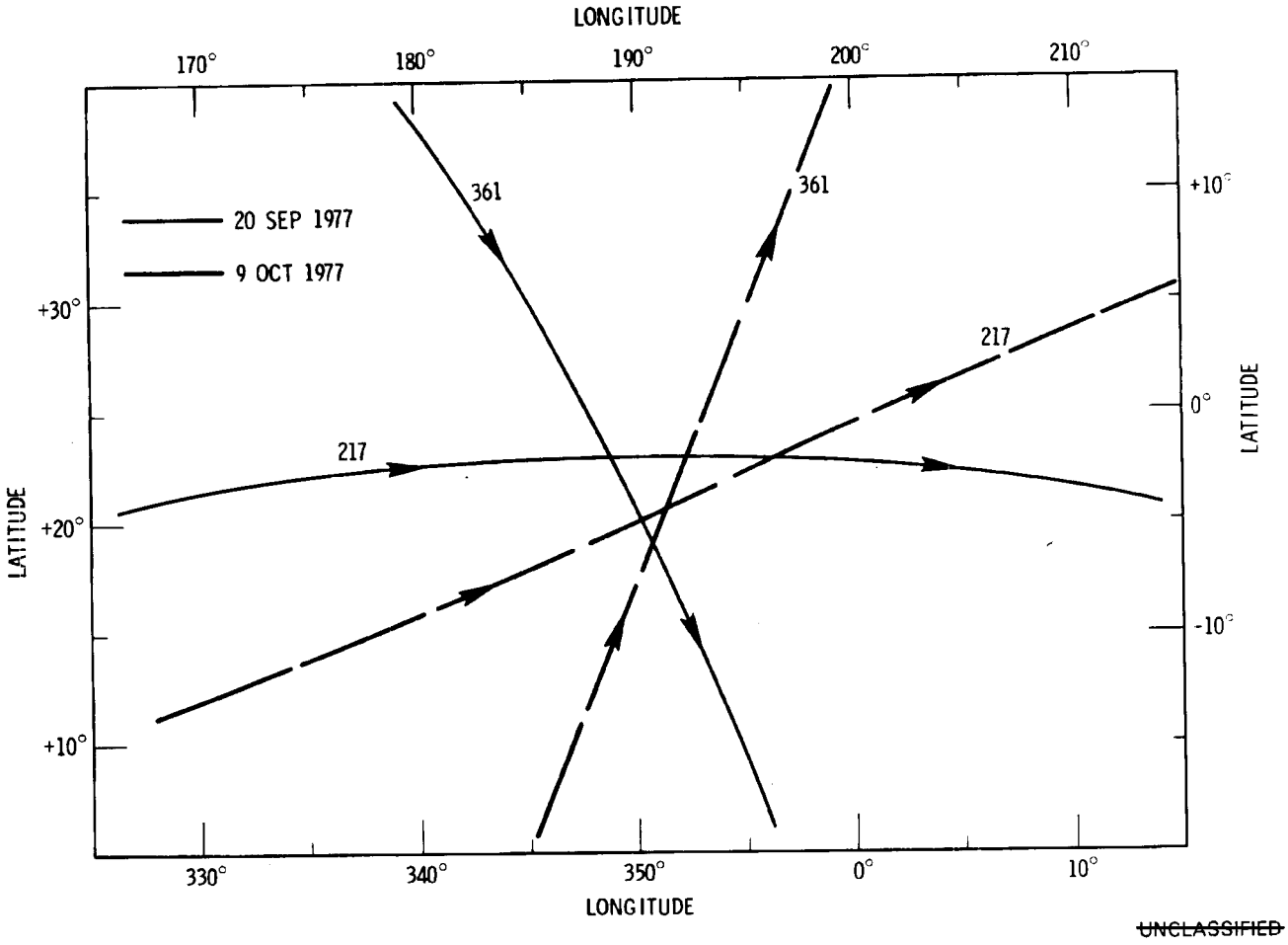
LONGITUDE
170°
180°
190°
200°
210°
361
361
20 SEP 1977
9 OCT 1977
+30°
217
217
+20°
+10°
LATITUDE
+10°
0°
-10°
LATITUDE
330°
340°
350°
0°
10°
LONGITUDE
UNCLASSIFIED

Figure 3

Table 4
HEAO A4 Detector Properties (U)

Name	No. in Inst.	Area (cm^2)	Field of View (degrees FWHM)	Normal Energy Range
High Energy Detector (HED)	1	120	43 (circular)	0.2 - 10 MeV
Medium Energy Detector (MED)	4	42	16 (circular)	0.08 - 2 MeV
Low Energy Detector (LED)	2	103	1.7 × 20 (box)	0.01 - 0.2 Mev
Particle Monitor	3	1 cm dia sphere	Omnidirectional	Protons >20 MeV >60 MeV >100 MeV; Electrons >1 MeV >6 MeV >20 MeV

~~UNCLASSIFIED~~

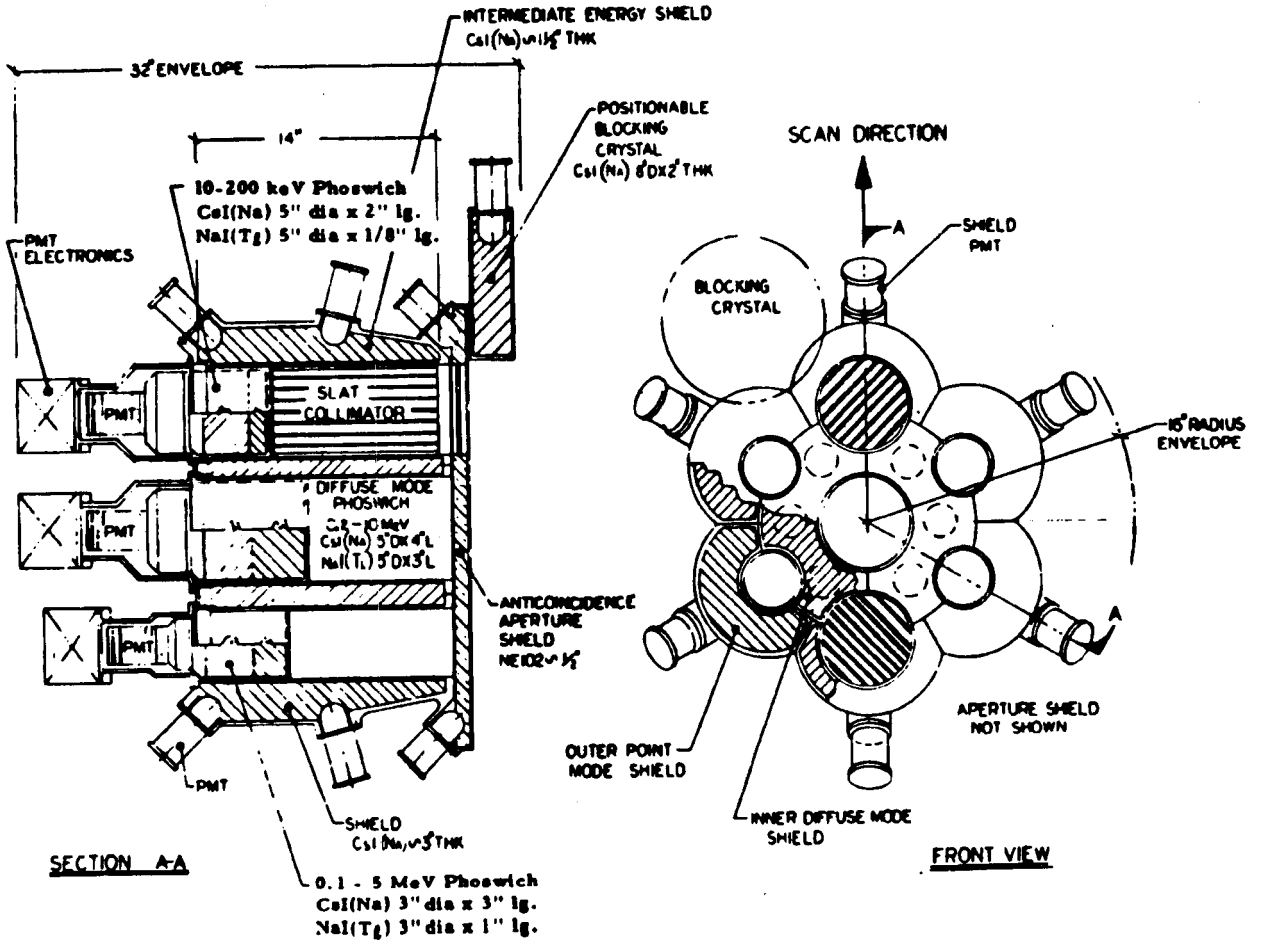

~~UNCLASSIFIED~~

Figure 4

~~(U)~~ The detectors fall into three categories according to the energy ranges in which they are used. In the center is the single high energy detector (HED), operating in the range 0.2-5.5 MeV. Surrounding the HED are six other detectors whose circular apertures can be seen in Figure 4. The four smaller apertures are for the medium energy detectors (MED), which operate in the 0.08-2.0 MeV range, and the remaining two are for the low energy detectors (LED), which operate in the 0.01-0.2 MeV range. The LEDs are furnished with metallic slats which limit the field of view (FOV) to 1.7o x 20o full width at half maximum (FWHM) boxes. The boxes of the two detectors are crossed. The MEDs and the HED have circular FOVs of FWHM 16o and 43o respectively. The FOVs are shown in Figure 5.

~~(U)~~ The signals from the detectors are processed by discriminators, pulse height analyzers (PHA), and pulse shape analyzers. Each detector is equipped with its own PHA so that 64 (LED) or 512 channel (MEDs and HED) energy loss spectra can be obtained. These dedicated PHAs are supplemented by a roving PHA which can obtain spectra from a command-selected detector. The roving PHA provides additional data handling capacity for rapid spectral analysis. For observations of short duration, the PHAs may not have sufficient time to accumulate full spectra or the total event count may be too low for utilization of the PHA resolution. In such cases rough energy spectra may be obtained by using the detector discriminators. Each detector is equipped with an upper and lower level discriminator (ULD and LLD) with the function of selecting events in a specific energy range for analysis. Since events having energy loss above the LLD and ULD triggering levels are counted and the totals telemetered, crude pulse height spectra may be obtained. The energy ranges in Table 4 correspond to the LLD and ULD settings. The LLD settings can be changed by command, so the

HEAO A-4 Instrument Fields of View

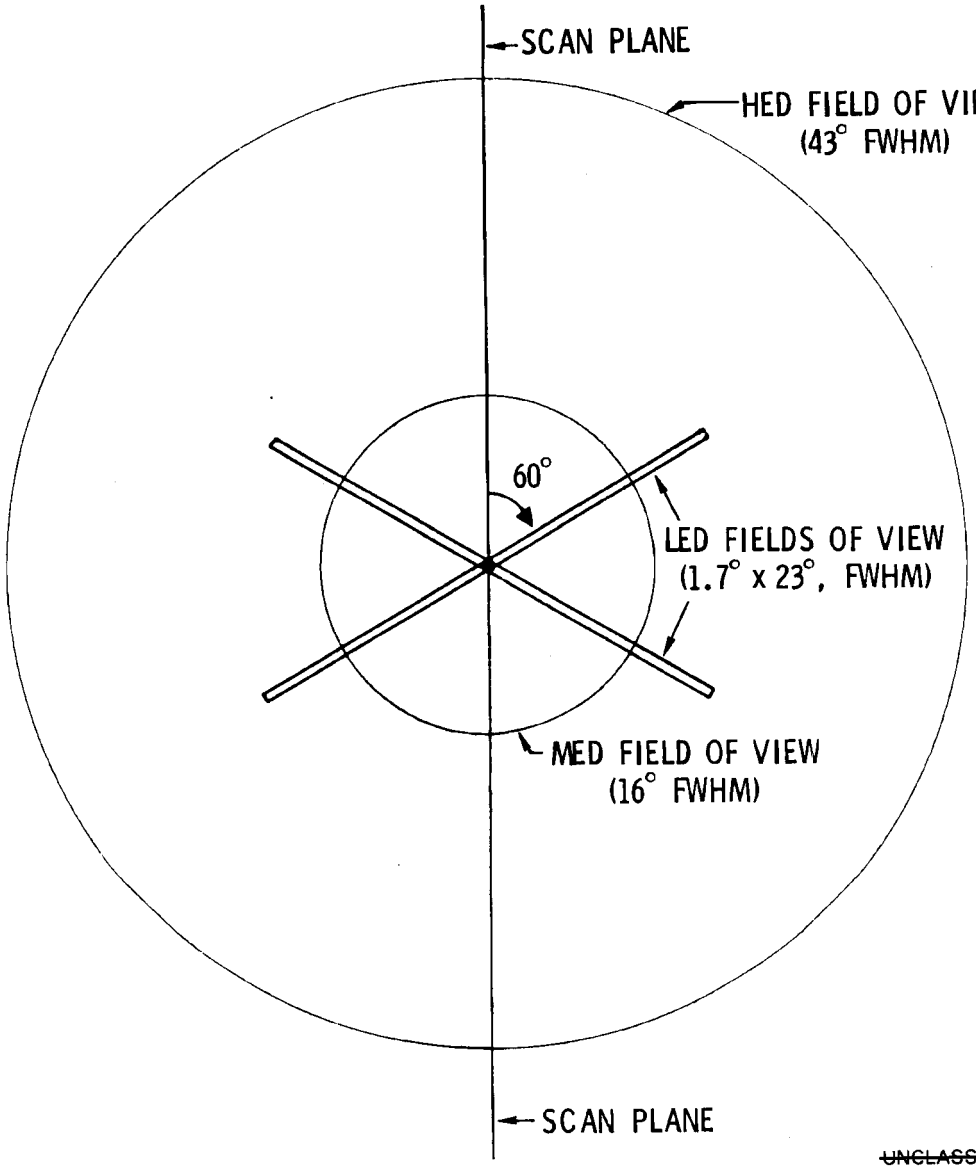

~~UNCLASSIFIED~~

Figure 5

energy ranges in the table can be varied to some degree. The HED range is divided into two parts by an intermediate level discriminator (ILD) set at 1-2 MeV. This allows additional spectral information to be obtained.

~~(S)~~ The ability of the HEAO A-4 detectors to detect the RORSAT gamma rays can be calculated from the detector geometry and the distance between HEA and the target vehicle. In Figure 6 the HEAO-COSMOS 954 range is plotted as a function of time for the two encounters in Figure 3.

(b)(1),1.4
(c)

The encounter durations were 80 and 110 seconds at the threshold of detectability. In reality the encounters would have been shorter because the target vehicle would not stay in the center of the detector field.

~~(S)~~ The CsI(Na) shields that surround the detectors are themselves very large area quasi-omnidirectional detectors. Such shields might be useful in detecting nuclear materials from space. However, shields were subject to very large background counting rates due to charged particles and cosmic X-rays and gamma rays. A calculation has shown that despite the high source counting rates the background rates in the HEAO A-4 detection shields were so high that the shields were not useful for detection of satellite-borne nuclear material.

~~(U)~~ Celestial γ-ray sources or sources fixed on or near the earth could give rise to false events in the HEAO-1 detectors. These events must be eliminated from consideration.

~~(S)~~ Celestial sources have signatures to distinguish them from the RORSAT nuclear reactors. Most obvious is that they were not detected at the times the RORSATs were detectable because at such times the earth occults the sky.

(b)(1),1.4
(c)

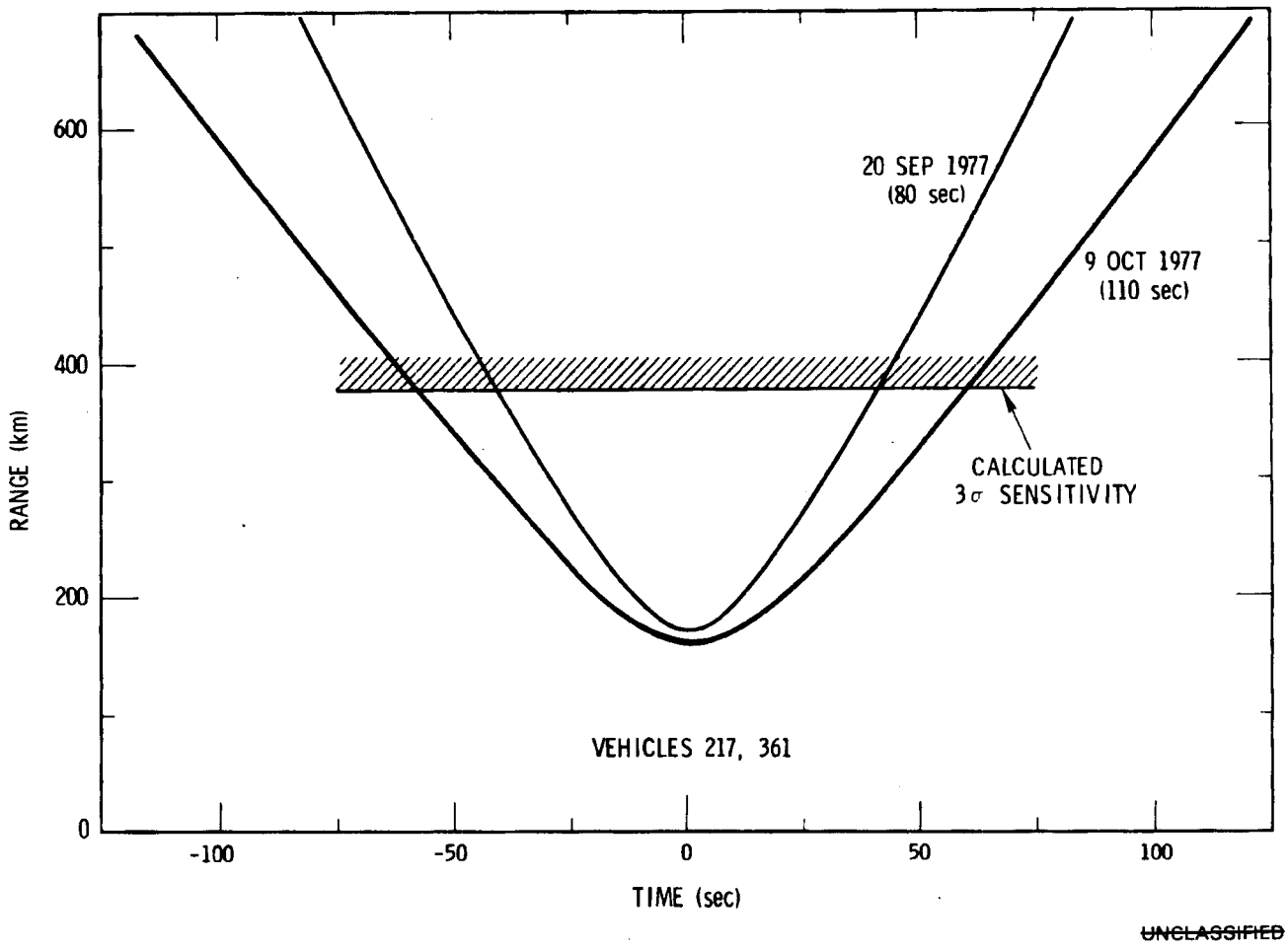
600
400
200
0
RANGE (km)
20 SEP 1977
(80 sec)
9 OCT 1977
(110 sec)
CALCULATED
3σ SENSITIVITY
VEHICLES 217, 361
-100
-50
0
50
100
TIME (sec)
UNCLASSIFIED

Figure 6

Furthermore, because the HEAO-1 spin axis direction changed very slowly a celestial source was detected on many satellite rotations. Figure 7 illustrates this. In the LED (D3 and D6) and MED (D2, D4, and D5) data the celestial source Cyg X-1 was repeatedly observed at intervals of 70 and 105 minutes (apparently the satellite spin period at this time was 35 minutes). The source was not observed on every rotation because of earth occultation (see "EARTH OCCULT" at bottom) and because the detectors were turned off when the satellite was in the South Atlantic Anomaly. A celestial source observation was generally longer than a RORSAT observation because the duration of the former was set by the time required for the satellite rotation to scan the detector field of view (43° FWHM for the HED and 16° FWHM for the MEDs) over the source at a spin rate of about 12 degrees per second. Finally, as noted above, the spectrum of gamma rays from a nuclear reactor is different from a celestial gamma ray source spectrum. Thus, a celestial gamma ray source is readily distinguishable.

~~(S)~~ To eliminate fixed sources on or near the earth we rely on the rarity of such events. The satellite-satellite encounters are so infrequent and so predictable that the likelihood of an earthbound event mimicking a satellite encounter is extremely small. For the two positive detection events to be discussed below, HEAO-1 was above Timbuktu and the Bahamas.

B. EVENTS ~~(U)~~

~~(S)~~ ADCOM orbit elements were used to calculate all encounters between HEAO-1 and COSMOS 952 and COSMOS 954 for which the minimum range was less than 500 km. Table 5 summarizes the results of these computations. HEAO data were analyzed with initial concentration on the twenty-three encounters having range less than 200 km. For three of these encounters the HEAO A-4 detectors were off. From the remaining 20 encounters two positive detections have been

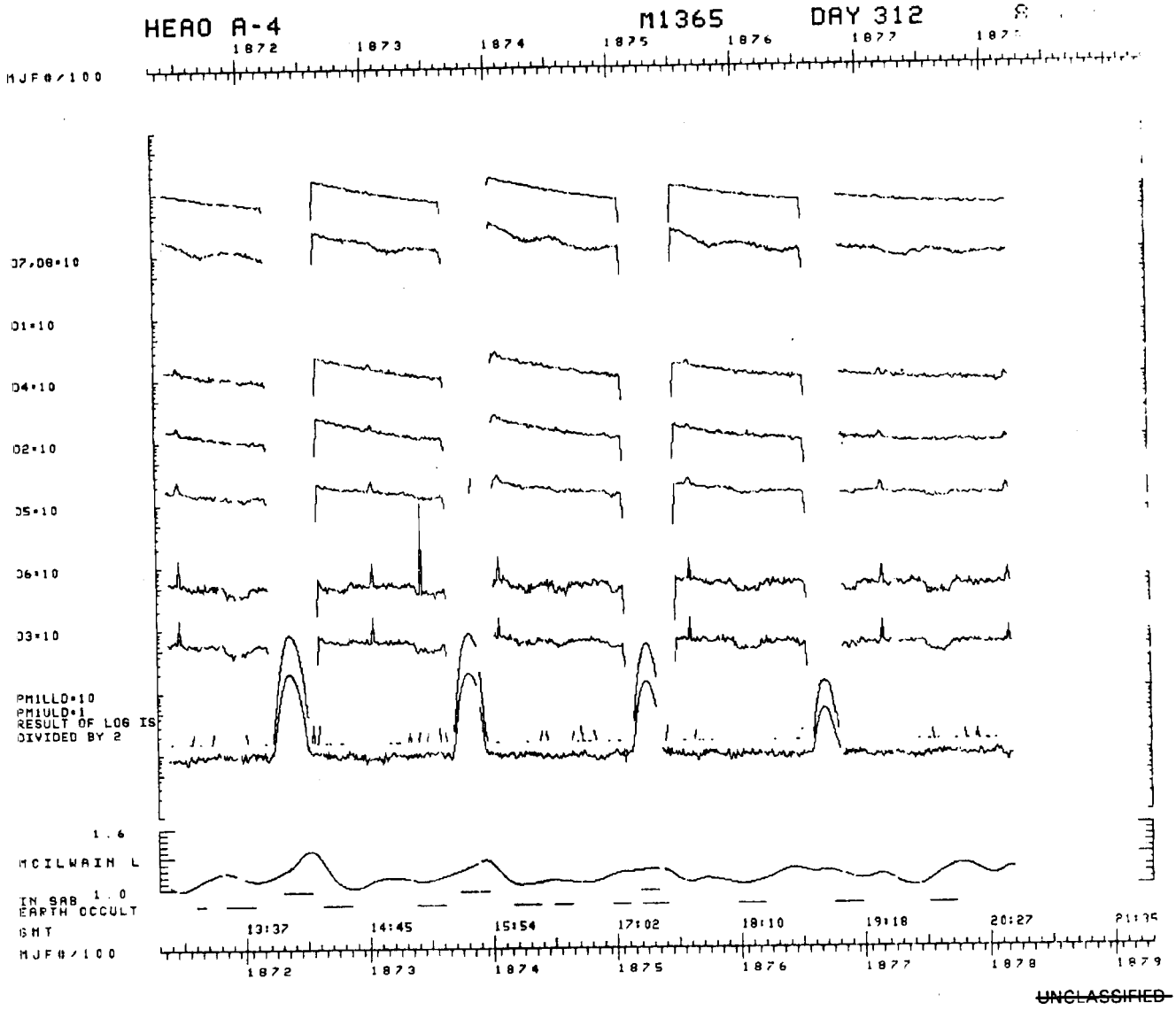
HEAO A-4
M1365
DAY 312
1872
1873
1874
1875
1876
1877
1878
MJF0/100
07,08*10
01*10
04*10
02*10
05*10
06*10
03*10
PM1LLO*10
PM1ULO*1
RESULT OF LOG IS
DIVIDED BY 2
1.6
MCILWAIN L
IN SAB 1.0
EARTH OCCULT
GMT
13:37
14:45
15:54
17:02
18:10
19:18
20:27
1879
UNCLASSIFIED

Figure 7

Table 5
Encounters (U)

	HEAO-1/COSMOS 952	HEAO-1/COSMOS 954
160 km ≤R≤ 200 km	3	20
20 km ≤ **R**≤ 500 km	11	79
Total R ≤ 500 km	113	

*R = minimum range.

~~SECRET~~

established. Subsequent analysis of the data from the more distant encounters have revealed no further events. The two events occurred on December 26, 1977 at 0113 UT, and on January 11, 1978, at 1557 UT. We discuss these events and their analysis below.

~~(S)~~ The January 11 event provided better data than did the December 26 event, so it will be discussed first. Although the minimum range was slightly larger for the January 11 event, the target passed through the detectors' fields of view at close range. The encounter is shown in Figure 8. The directions of the HEAO-target vectors and the A-4 HED pointing vectors are shown at three times denoted a, b, and c. The ranges at these three times were 320 km, 199 km, and 312 km respectively. The oval shape is the envelope swept out by the HED FWHM field of view between time a and time c. One can see that the target passed very near the center of the FOV at some time between 1557:38 UT and 1558:19 UT. The maximum HED response occurred at 1557:53 when the range was 216 km and the target was 11.6° off axis. The maximum MED response was at 1557:58 when the range was 229 km and the target was 9.7° off axis. These maximums occur at different times because the response includes an angle factor and a distance factor. Because the MEDs have a smaller FOV than the HEDs, their response is more sensitive to the angular factor.

~~(U)~~ Figure 9 shows the HED and MED discriminator counts during the 11 January event as a function of time. Each data read-out interval is 10.24 seconds. The source spectrum was obtained from the data by performing the following sum:

$$F_{200}(j) = \frac{1}{10.24\,(m + 1 - n)} \frac{\sum_{i=m}^{n} \frac{C(i,j) - B(i,j)}{R_{200}(i,j)\,\sigma^2(i,j)}}{\sum_{i=m}^{n} \frac{1}{\sigma^2(i,j)}} \qquad (1)$$

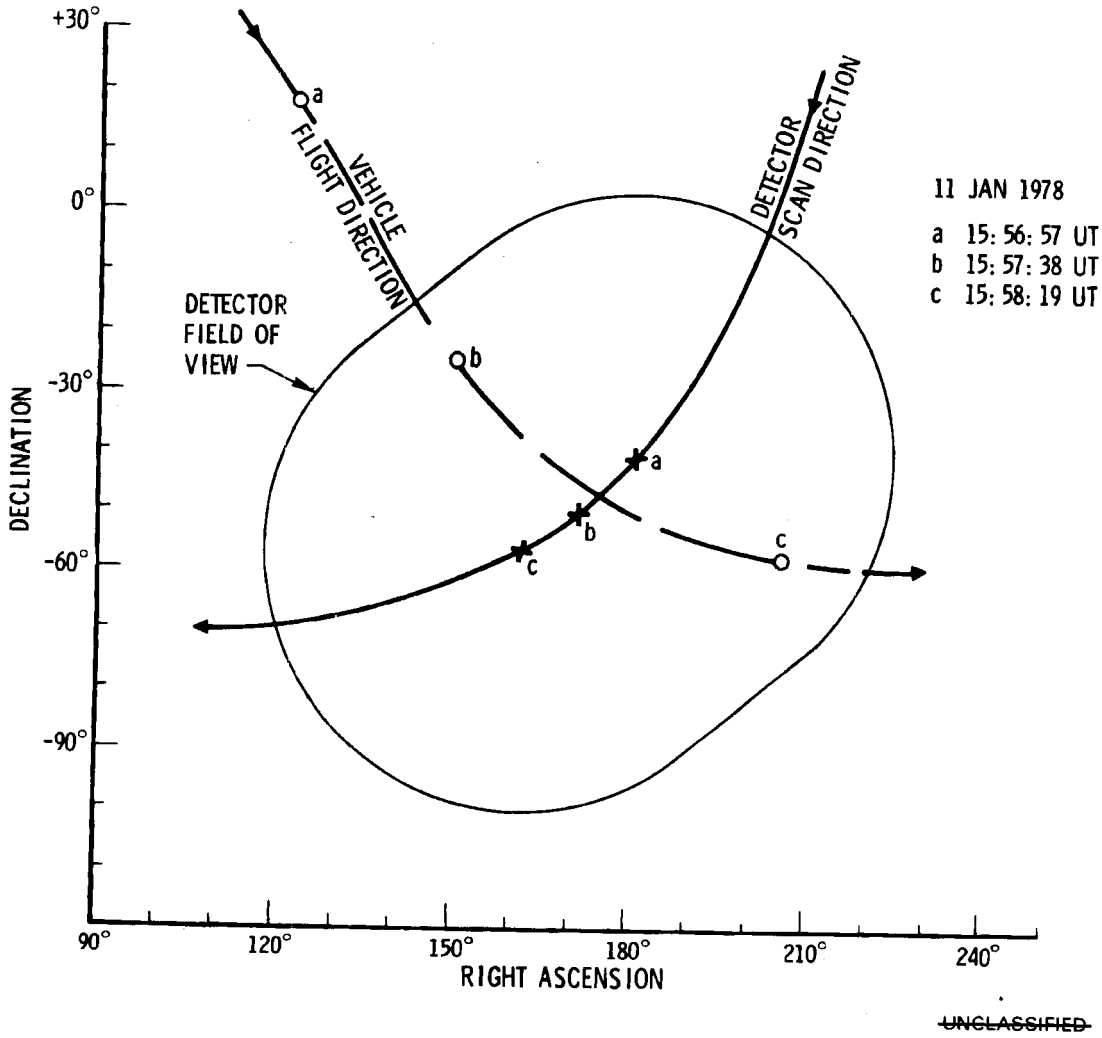
+30°
0°
-30°
-60°
-90°
DECLINATION
90°
120°
150°
180°
210°
240°
RIGHT ASCENSION
VEHICLE FLIGHT DIRECTION
DETECTOR SCAN DIRECTION
DETECTOR FIELD OF VIEW
a
b
c
11 JAN 1978
a 15: 56: 57 UT
b 15: 57: 38 UT
c 15: 58: 19 UT
~~UNCLASSIFIED~~

Figure 8

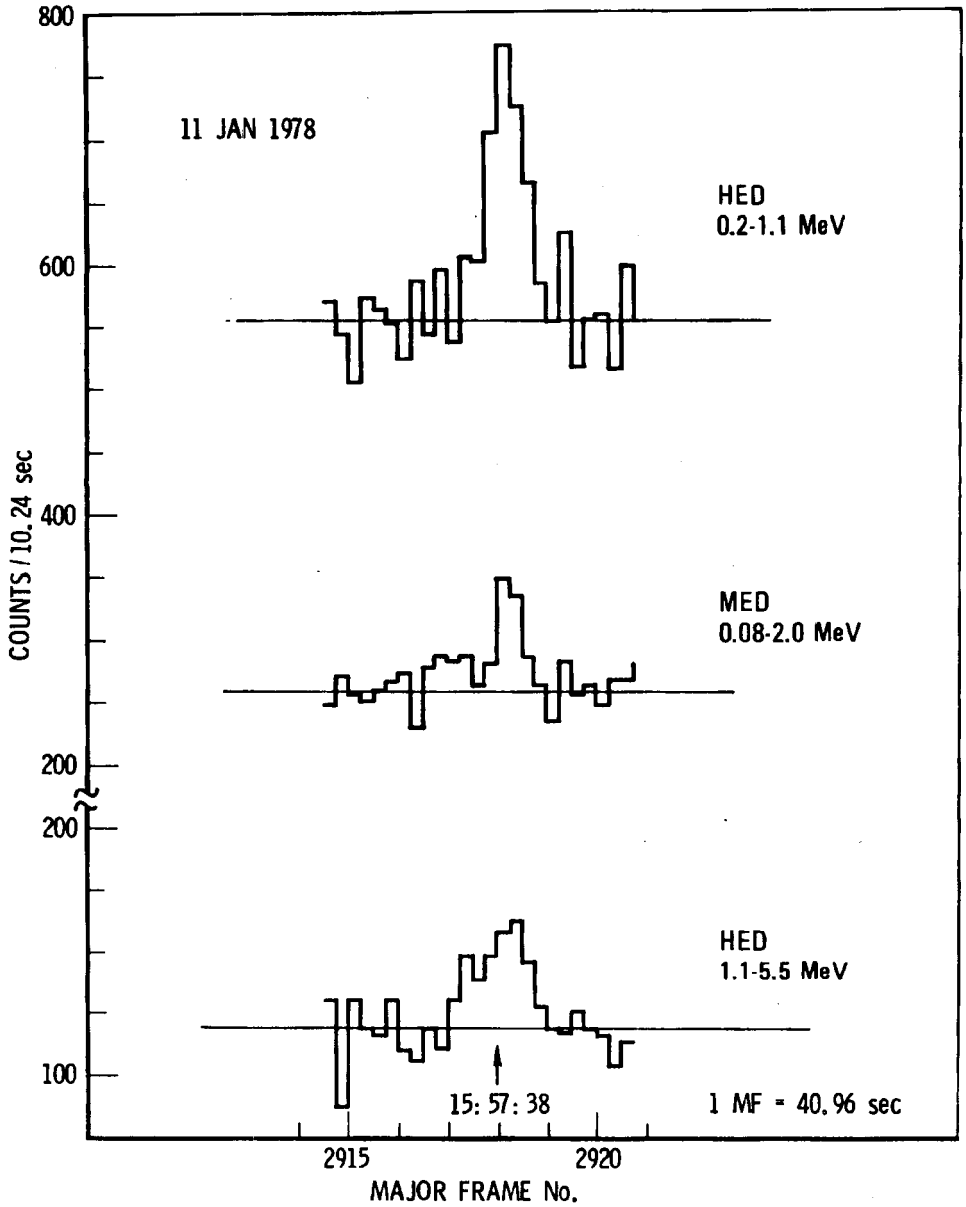

~~UNCLASSIFIED~~

Figure 9

where F_{200} (j) is the flux in energy channel j (photons $-cm^{-2}-s^{-1}$) at a range of 200 km, C(i, j) is the counts recorded in channel j during interval i, B(i, j) is the channel j background level, $\sigma(i, j)$ is the standard deviation of $(C(i, j) - B(i, j))/R_{200}(i, j)$, and

$$R_{200}(i, j) = \frac{(\theta_j - \theta_i)}{\theta_j} \left(\frac{200}{r_i}\right)^2 \epsilon_j A_j. \quad (2)$$

In equation (2) θ_j is the FWHM of the detector response in channel j, θ_i is the off-axis angle of the source, r_i is the range during interval i, ϵ_j is the detector efficiency in channel j, and Aj is the detector area in channel j (i.e., the HED or MED area, whichever is appropriate to channel j). The data in Figure 9 are from the MED and HED discriminator print-outs; the PHA data will be discussed below.

(8) Figure 10 shows the spectrum derived from the data in Figure 9 by using the procedure described in the previous paragraph. Each plotted point is the integral photon flux, at a range of 200 km, above the energy at which the point is located. The MED point therefore includes both MED and HED flux, and the lower HED point is derived from data in both HED channels. In converting the discriminator fluxes to integral fluxes a standard spectral shape (to be discussed below) was assumed. Specifically, the MED point included all of the MED flux plus the HED upper channel flux multiplied by a factor to convert 1.1-5.5 MeV flux to flux above 2 MeV. The HED LLD point includes the LLD flux plus the ILD (intermediate level discrimination, 1.1 MeV) flux times a factor (very close to 1) to convert 1.1-5.5 MeV flux to flux above 1.1 MeV. The source was not detected in the LED. This is not surprising; a modest amount of shielding

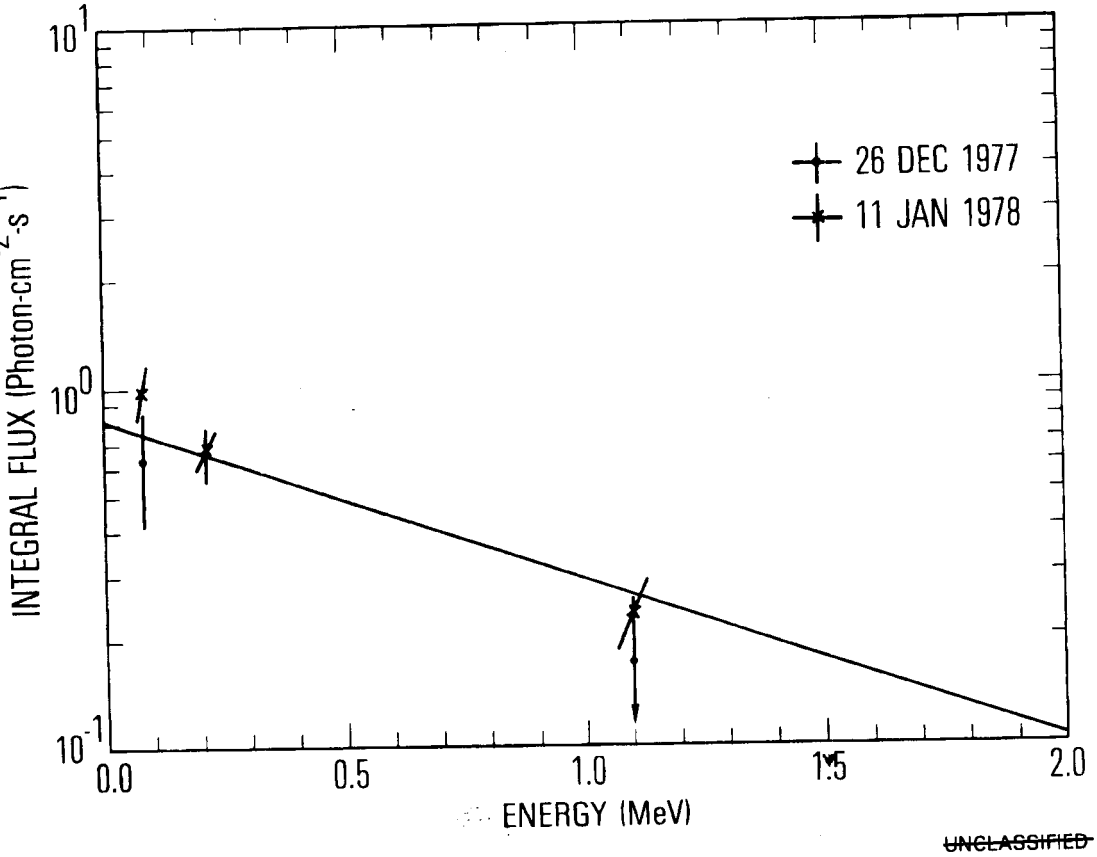
10^1
10^0
10^{-1}
INTEGRAL FLUX (Photon-cm^{-2}-s^{-1})
26 DEC 1977
11 JAN 1978
0.0
0.5
1.0
1.5
2.0
ENERGY (MeV)
~~UNCLASSIFIED~~

Figure 10

around the reactor would attenuate low energy gamma rays. Also shown in Figure 10 are the discriminator data from the 26 December event.

~~(S)~~ The line in Figure 10 is an exponential fission spectrum fitted to the data. Keepin (1965) discusses the delayed gamma ray spectrum as a function of time following fission. For a period of very roughly 1000 seconds following fission the number spectrum can be approximated by the form $A_I e^{-1.026E}$ where A_I is a constant and E is the gamma ray energy. During this time most of the delayed gammas are emitted. The line in Figure 10 is the best fit, obtained by varying A_I, to all of the discriminator data from both events. For the spectrum in Figure 10, $A_I = 0.818$. For the 11 January data alone, $A_I = 0.850$. The fits are good evidence that COSMOS 954 carried a reactor, and will allow us to estimate the power output.

~~(U)~~ PHA data were also obtained for the 11 January event. A spectrum derived using equations (1) and (2) is shown in Figure 11. Note that here we plot differential flux in photon $-cm^{-2}\ s^{-1}\ MeV^{-1}$. The fit is to the form $A_D e^{-1.026E}$. A_D should be related to A_I by $A_D = A_I \times 1.026$. We find $A_D = 0.805$, which agrees with AI for January 11 to an accuracy of about eight percent. The fit to the differential spectrum had a χ^2 statistic of 14.45 for 13 degrees of freedom. The probability of obtaining a greater χ^2 by chance is 35%; therefore the fit is acceptable.

~~(U)~~ The observing conditions for the December 26 event were not as favorable as those for the January 11 event. The range was large when the off-axis angle was smallest. The maximum response in both detectors occurred at 0113:46 UT when the range was 355 km and the angle was 2.4^o. The geometry is shown in Figure 12.

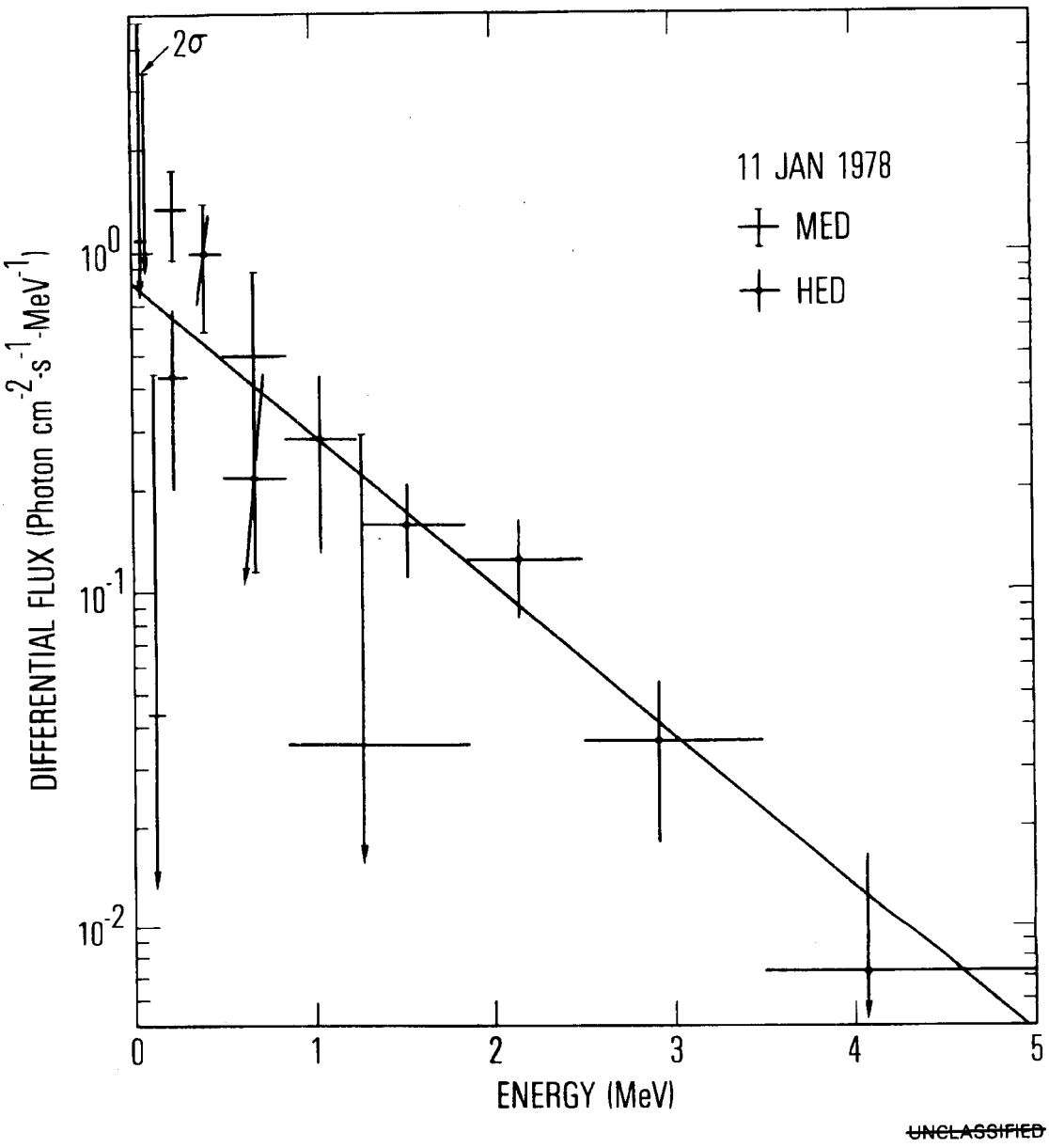
2σ
11 JAN 1978
MED
HED
DIFFERENTIAL FLUX (Photon cm^{-2}-s^{-1}-MeV^{-1})
10^{0}
10^{-1}
10^{-2}
0
1
2
3
4
5
ENERGY (MeV)
~~UNCLASSIFIED~~

Figure 11

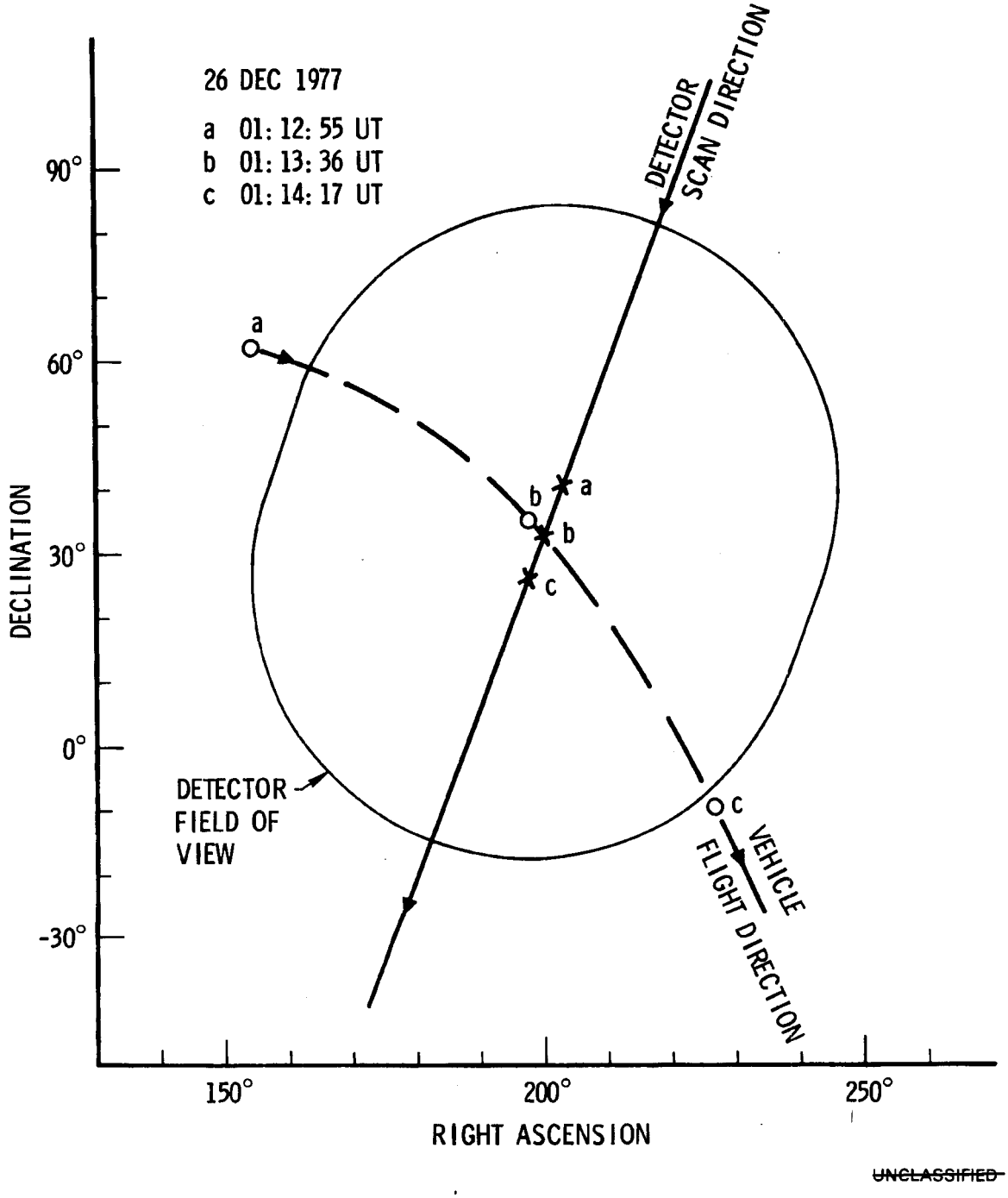
26 DEC 1977
a 01: 12: 55 UT
b 01: 13: 36 UT
c 01: 14: 17 UT
DETECTOR SCAN DIRECTION
90°
60°
30°
0°
-30°
DECLINATION
a
b
c
DETECTOR FIELD OF VIEW
VEHICLE FLIGHT DIRECTION
150°
200°
250°
RIGHT ASCENSION
UNCLASSIFIED

Figure 12

~~(U)~~ Figure 13 shows the counting data for the December 26 event. There is no question that the source was detected in all three channels. These data were analyzed with the same procedures as for the January 11 event. The integral spectrum data are plotted in Figure 10. The best fit to the 26 December data alone had $A_I = 0.730$.

~~(U)~~ PHA data were also obtained for the 26 December event. These are shown in Figure 14, along with the best fit spectrum of the form $A_D e^{-1.026E}$. The best fit is obtained for $A_D = 0.871$, a value about 16% above 1.026 A_I for 26 December and 8% above A_D for the 11 January event. The χ^2 statistic is 9.36 for 13 degrees of freedom, with a χ^2 probability of about 75%. Again the fit is acceptable.

~~(S)~~ As a final step in the data analysis, all of the differential spectrum data for the two events were combined and fitted to the standard fission delayed gamma ray spectrum. The best fit spectrum had $A_D = 0.824$, which corrsponds to $A_I = 0.803$, in good agreement with $A_I = 0.818$ obtained from the integral spectra. The χ^2 statistic for the combined fit is 24.50 for 28 degrees of freedom, giving a χ^2 probability of 70%. Again the fit is acceptable. The excellent fit obtained by combining data from two separate encounters and from two separate detectors having different fields of view testifies to the high quality of the ephemeris and attitude data for the two vehicles.

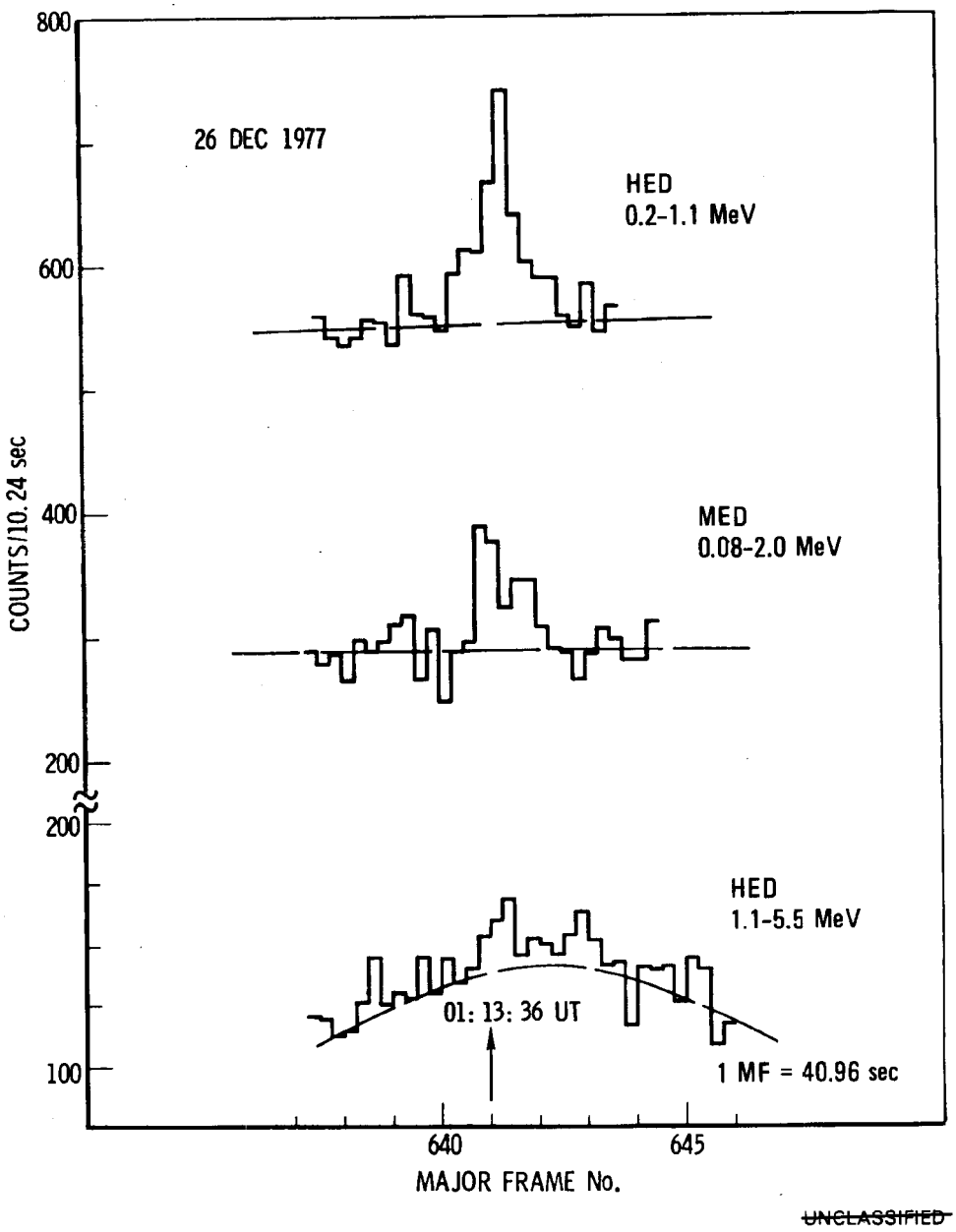
800
600
400
200
200
100
26 DEC 1977
HED
0.2-1.1 MeV
MED
0.08-2.0 MeV
HED
1.1-5.5 MeV
01: 13: 36 UT
1 MF = 40.96 sec
COUNTS/10.24 sec
640
645
MAJOR FRAME No.
~~UNCLASSIFIED~~

Figure 13

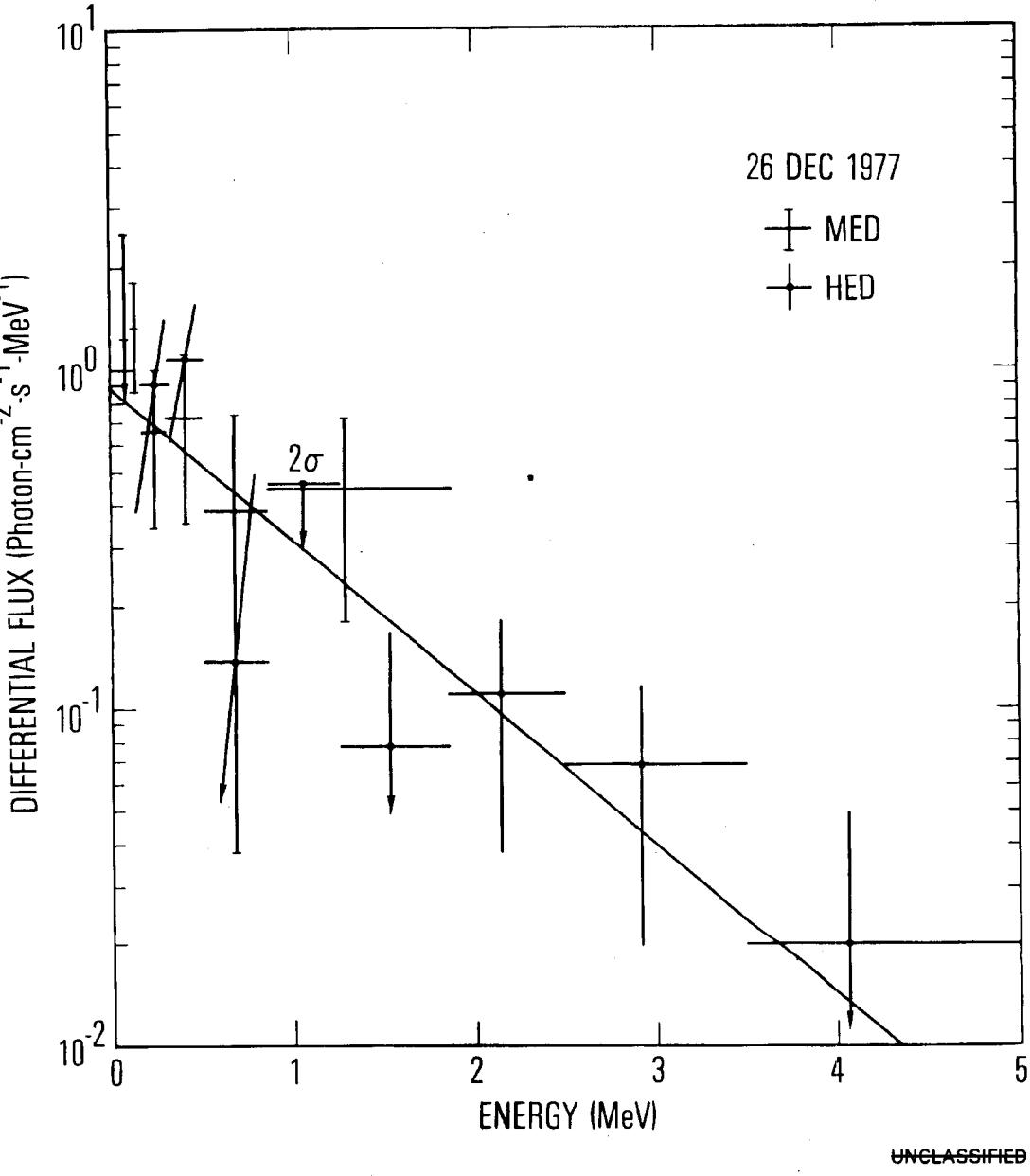
26 DEC 1977
MED
HED
2σ
DIFFERENTIAL FLUX (Photon-cm^{-2}-s^{-1}-MeV^{-1})
ENERGY (MeV)
10^{1}
10^{0}
10^{-1}
10^{-2}
0
1
2
3
4
5
UNCLASSIFIED

Figure 14

IV. HEAO-3 MEASUREMENTS ~~(U)~~

~~(U)~~ The HEAO-3 satellite carried three experiments, one being a high-resolution gamma-ray spectrometer designed to observe gamma-ray line-emission from astronomical objects. The principal investigator was Dr. Allen Jacobson of JPL. The sensor consisted of four germanium detectors, with a volume of approximately 100 cm^3 each, surrounded by a 6.6 cm thick CsI anticoincidence shield. The entrance aperture was actively shielded against charged particle penetration by a 0.35 cm thick plastic scintillator.

~~(S)~~ The instrument configuration is shown in Figure 15. Note that the CsI anticoincidence shield is segmented into four quadrants plus a collimator segment in front in order to provide some direction finding capability for photons not coming in the aperture. For present purposes this directionality is used to verify the fact that the gammas observed during close encounters come from the known direction of the RORSAT.

~~(S)~~ The HEAO-3 spun slowly, in much the same fashion as HEAO-1, cf. Figure 1. Thus in general the apertures of the germanium array did not point in the direction of the RORSAT. The shield effectiveness of the CsI ranged from substantially greater than an order-of-magnitude at 100 keV to less than a factor of 2 at 1.5 MeV. Therefore the best hope of seeing gamma-ray lines from the reactor which get through the shield and into the germanium detectors is in the MeV energy range. Two energy channels are used on each of the CsI shields; the lower level is $\sim$100 keV and the upper one $\sim$4 MeV. The charged particle detector thresholds are $\sim$200 keV and $\sim$2 MeV.

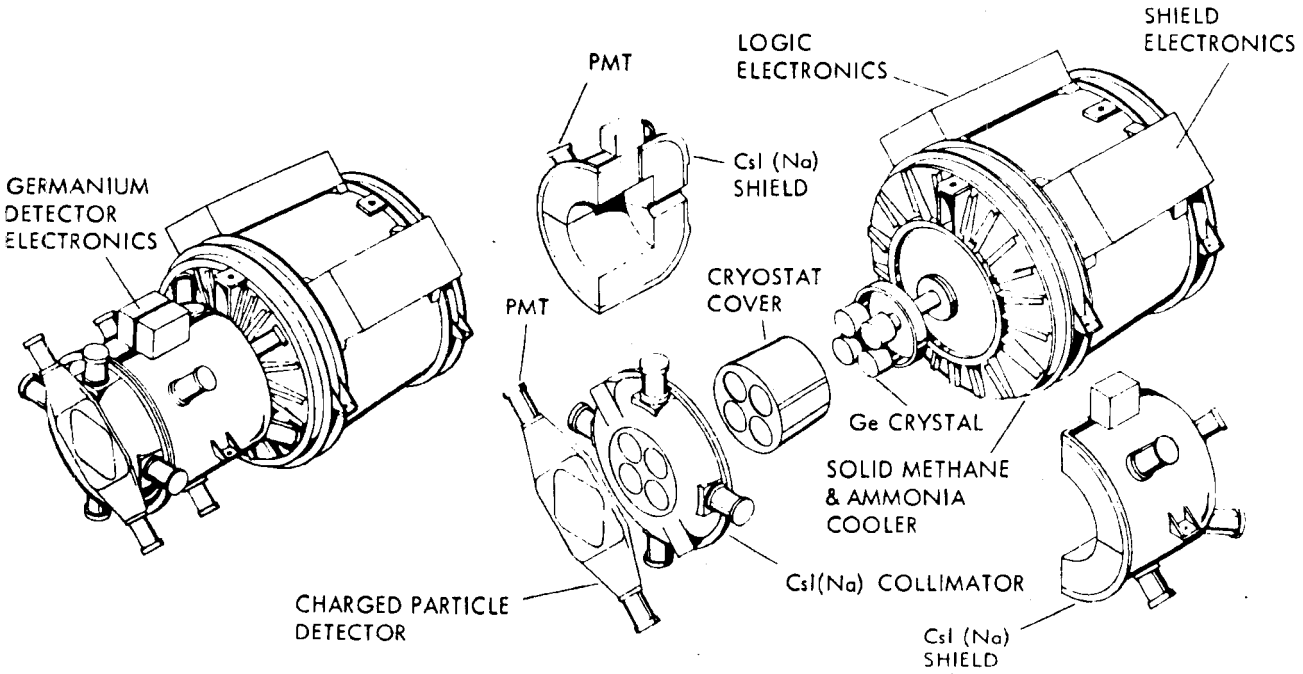

~~UNCLASSIFIED~~

Figure 15

~~(S)~~ An example of the data collected on day 156 around the time of a close RORSAT encounter is shown in Figures 16 and 17 for one of the four CsI side shields (S4) for the lower and upper energy channels, respectively. Count-rate is displayed vs time for a ∿3 hour period centered at the predicted time of closet approach to the RORSAT. Note there are periods when the count rates go abruptly to zero; this occurs when the satellite enters the region of the South Atlantic Anomaly. The experiment is deliberately turned off to prevent damage by the copious fluxes of energetic protons found there.

~~(S)~~ The presence of the RORSAT can be seen clearly as a spike in the count rates just following the predicted time of closest approach (21.82UT). The enhancement in the low-energy channel is 250 cps and in the high-energy channel is ∿20 cps. Two features are immediately apparent: the energy spectrum is hard as expected for a reactor, cf. Figure 10; the observed count rate corresponds to a flux of a few tenths of a $\gamma/(cm^2\text{-sec})$ as predicted for a 40 kW reactor, cf. Table A1. Shield S4 was directed most favorably towards the RORSAT and had the best signal. Shield S2 was directed oppositely and shows the weakest signal. Figure 18 gives the S2 low-energy channel display for the same time period as shown in Figures 16 and 17 for S4.

~~(U)~~ Figure 19 shows the data from the low-energy charged particle detector. The strong signal in this plastic scintillator is unexpected. Furthermore, the charged-particle detector consistently shows a strong signal during close approaches and not just during this one encounter. Its efficiency to photons is low and the predicted neutron flux (Table A1) is insufficient to account for the observed signal. At present this observation is not understood.

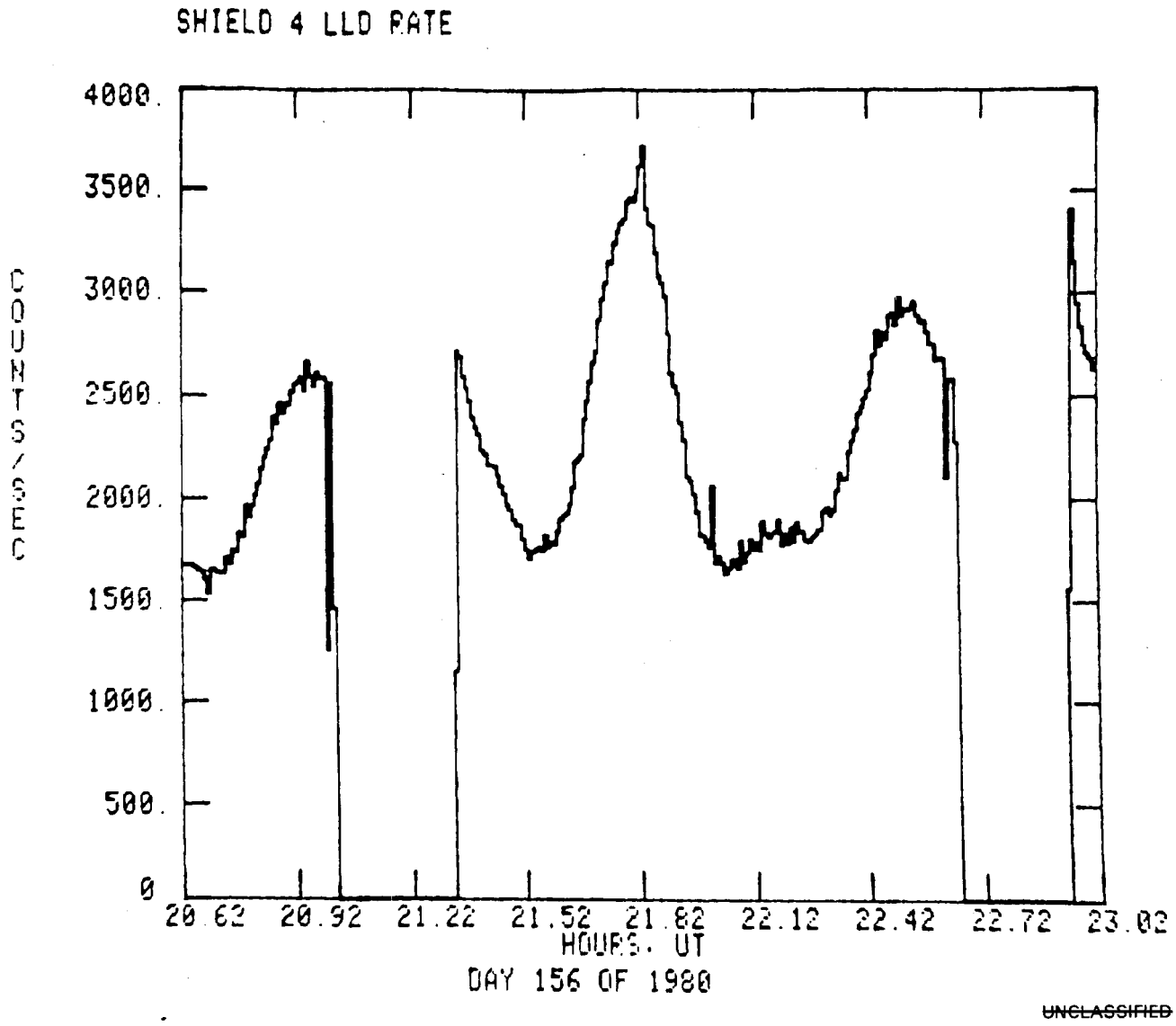
SHIELD 4 LLD RATE
4000.
3500.
3000.
2500.
2000.
1500.
1000.
500.
0
COUNTS/SEC
20.62
20.92
21.22
21.52
21.82
22.12
22.42
22.72
23.02
HOURS. UT
DAY 156 OF 1980
UNCLASSIFIED

Figure 16

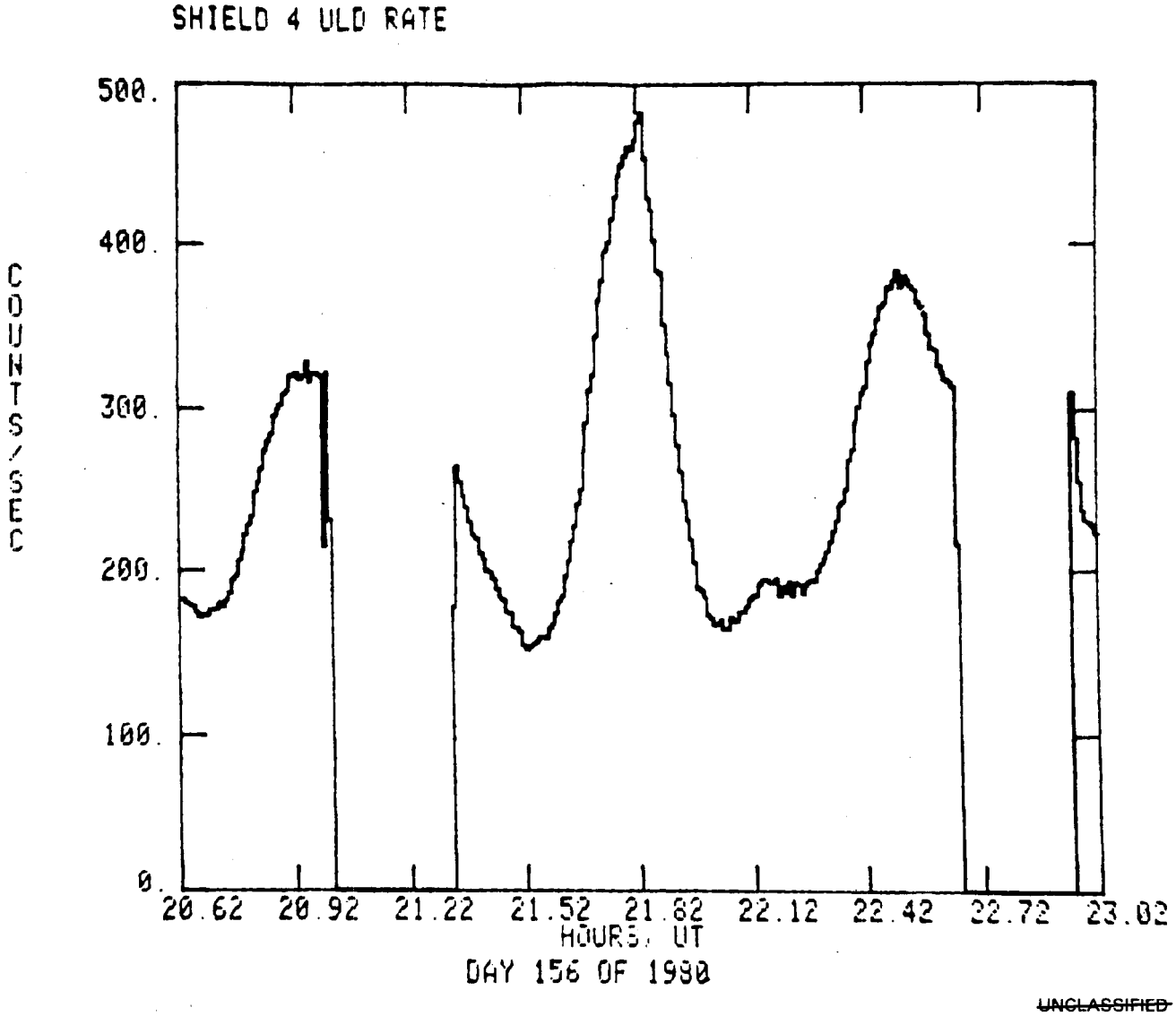
SHIELD 4 ULD RATE
500.
400.
300.
200.
100.
0.
COUNTS/SEC
20.62
20.92
21.22
21.52
21.82
22.12
22.42
22.72
23.02
HOURS, UT
DAY 156 OF 1980
UNCLASSIFIED

Figure 17

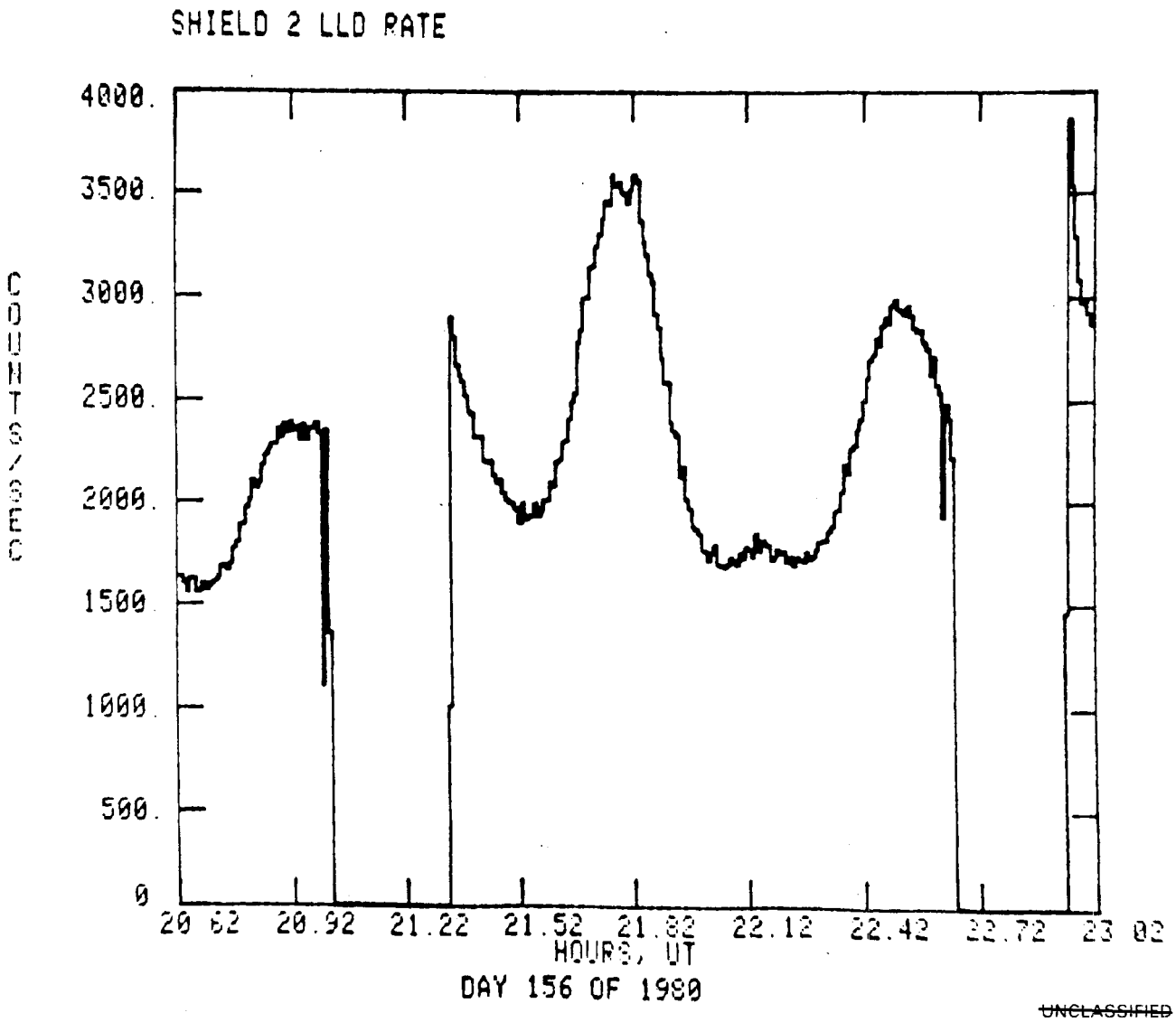
SHIELD 2 LLD RATE
4000.
3500.
3000.
2500.
2000.
1500.
1000.
500.
0
COUNTS/SEC
20.62
20.92
21.22
21.52
21.82
22.12
22.42
22.72
23.02
HOURS, UT
DAY 156 OF 1980
UNCLASSIFIED

Figure 18

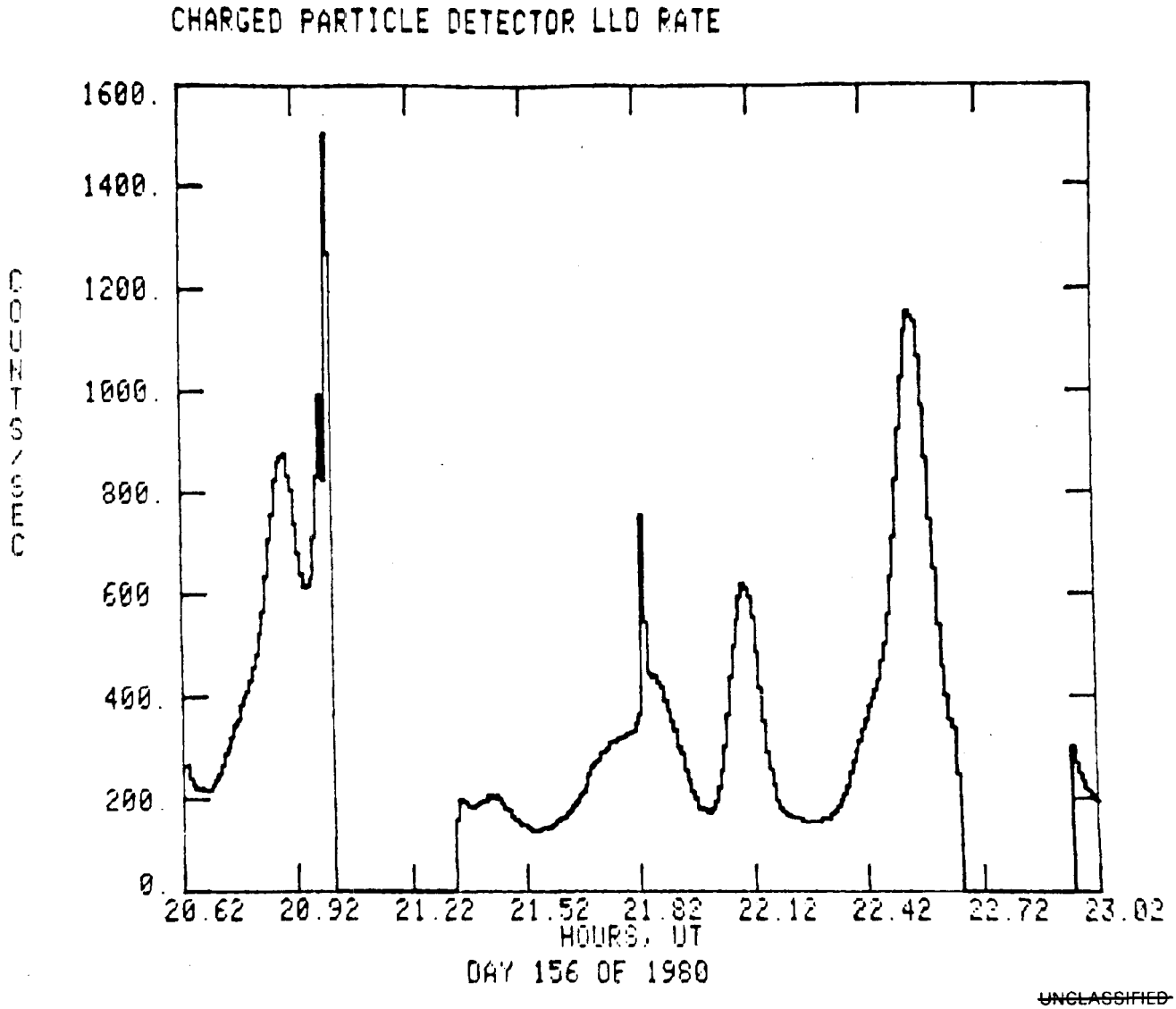
CHARGED PARTICLE DETECTOR LLD RATE
1600.
1400.
1200.
1000.
800.
600
400.
200.
0.
COUNTS/SEC
20.62
20.92
21.22
21.52
21.82
22.12
22.42
22.72
23.02
HOURS, UT
DAY 156 OF 1980
UNCLASSIFIED

Figure 19

~~(S)~~ Another set of encounter results is given in Figures 20 and 21 for day 134. On this day the germanium detectors were still cold, but unfortunately their fields of view were directed orthogonally to the direction to the RORSAT. The germanium data has been examined, and no lines resulting from gamma rays penetrating the shield are obvious. It is worthwhile to attempt a background subtraction but this has not been carried out yet. ~~(SECRET/NOFORN)~~ (REVIEW ON 20 JULY 2011)

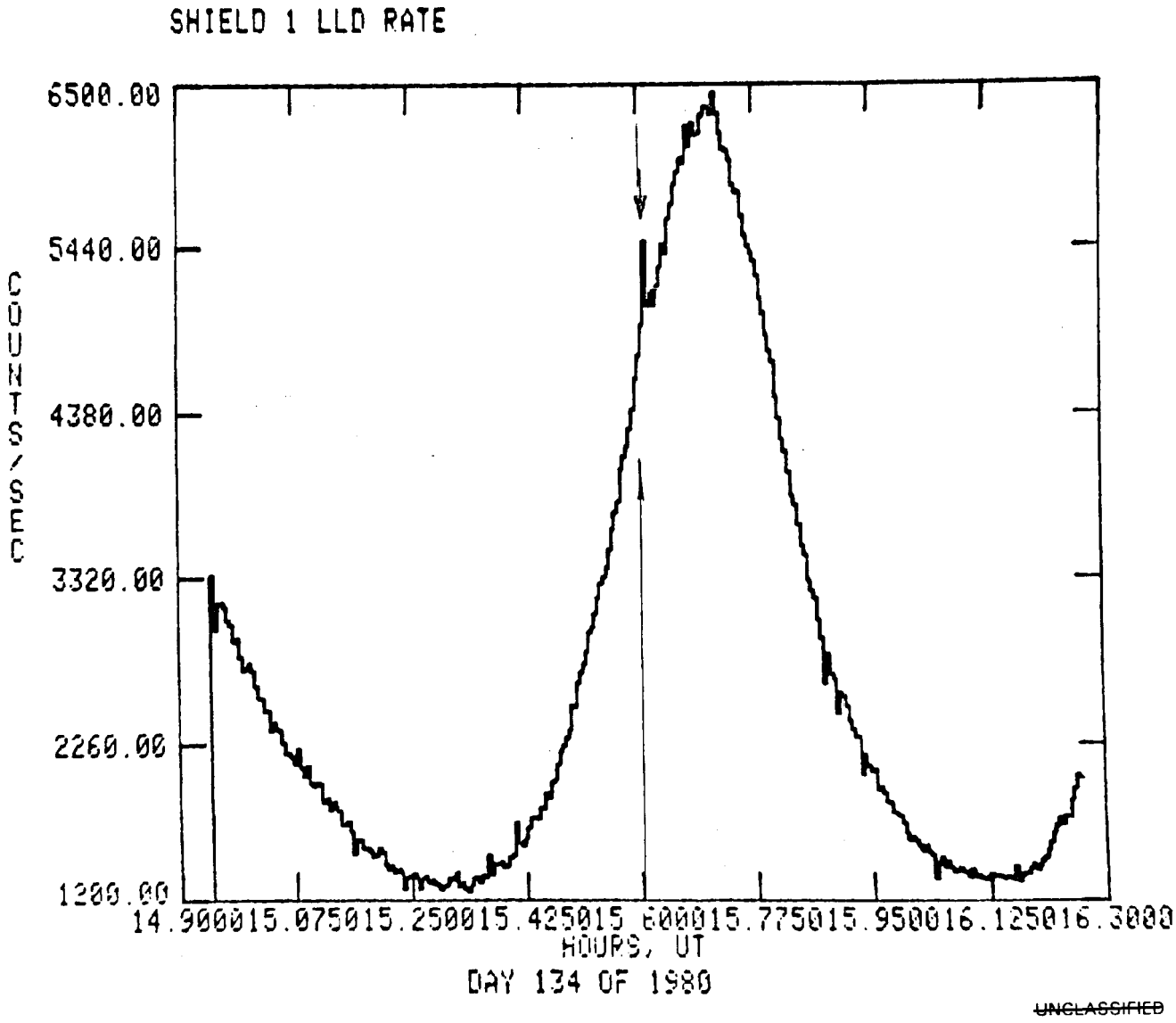
SHIELD 1 LLD RATE
6500.00
5440.00
4380.00
3320.00
2260.00
1200.00
COUNTS/SEC
14.900015.075015.250015.425015.600015.775015.950016.125016.3000
HOURS, UT
DAY 134 OF 1980
UNCLASSIFIED

Figure 20

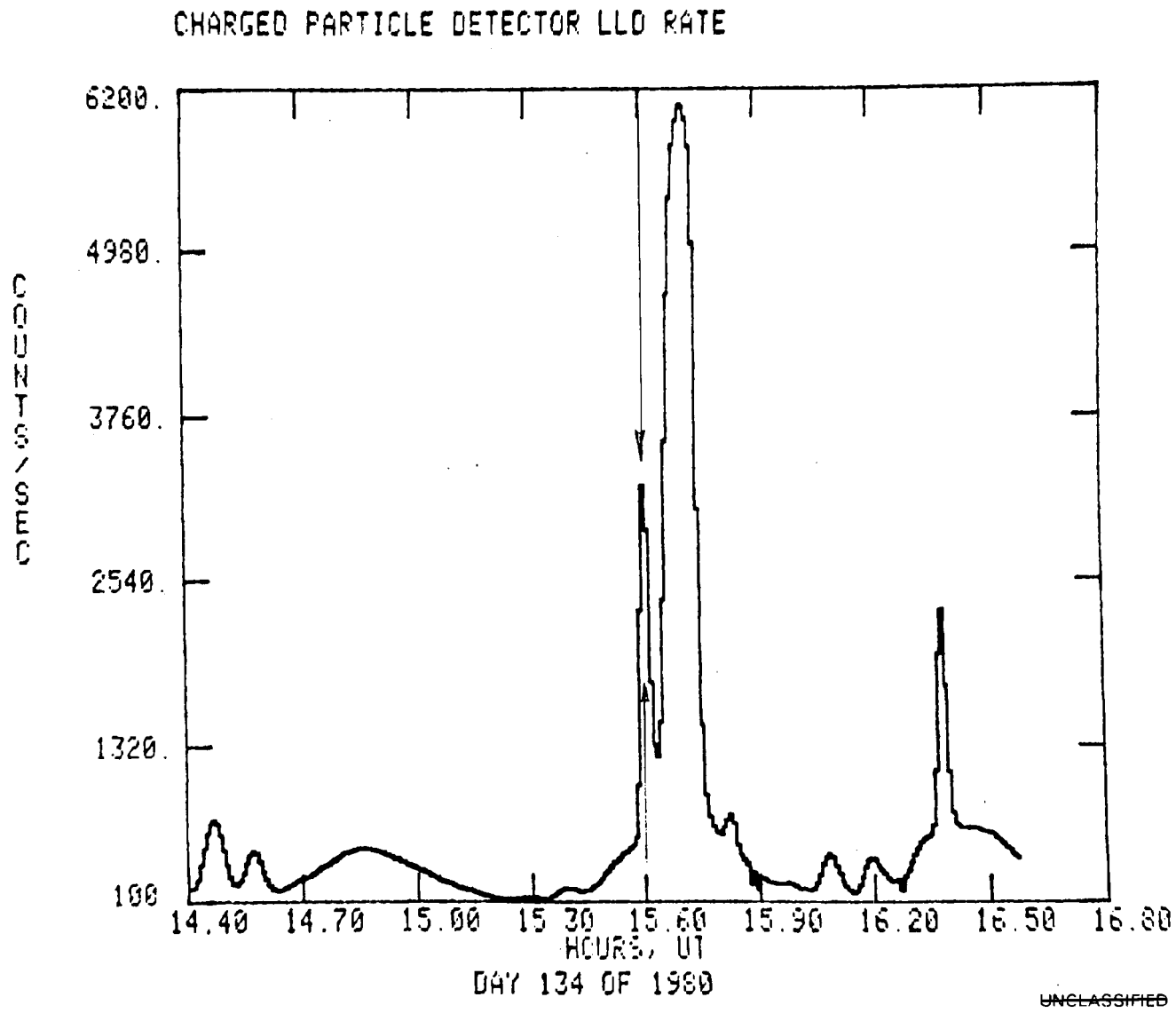
CHARGED PARTICLE DETECTOR LLD RATE
6200.
4980.
3760.
2540.
1320.
100
COUNTS/SEC
14.40
14.70
15.00
15.30
15.60
15.90
16.20
16.50
16.80
HOURS, UT
DAY 134 OF 1980
UNCLASSIFIED

Figure 21

APPEXDIX. ESTIMATE OF SIGNAL STRENGTH ~~(U)~~

~~(S)~~ The following parameters are assumed for the nuclear reactor aboard the RORSATs.

40 kW thermal power

235U fuel

Leakage of neutrons and gammas of 10%

Neutrons / fission, $\nu = 2.43$

Gammas / fission = 10

Energy / fission = 195 MeV

~~(U)~~ The number of fissions/second is given by

$$40 \times 10^3 \ \frac{\text{joules}}{\text{sec}} \times \frac{10^7 \ \text{ergs}}{\text{joule}} \times \frac{1}{1.6 \times 10^{-6}} \ \frac{\text{MeV}}{\text{erg}} \times \frac{1}{195} \ \frac{\text{fission}}{\text{MeV}} \qquad (1)$$

$$= 1.3 \times 10^{15} \text{ fissions/sec}$$

which yields the following neutron and gamma leakage:

3.1×10^{14} neutrons/sec

1.3×10^{15} gammas/sec

(2)

~~(S)~~ Assuming isotropy of emission, if s is the separation between the RORSAT and the satellite containing the detector(s), the flux at the detector as a function of range is given in Table A1.

Table A1
Signal Strength Estimate ~~(U)~~

s (km)	n/cm^2 sec	γ /cm^2 sec
1	2.5 (3)	1.0 (4)
10	25	100
100	0.25	1.0
150	0.11	0.46
180	0.076	0.32
200	0.062	0.26
220	0.051	0.21

~~SECRET~~

REFERENCES

Keepin, G. R. 1965, Physics of Nuclear Kinetics

(Reading, Massachusetts: Addison-Wesley), Chapter 5.

(b)(3):10 USC 424,(b)(3):50 USC 3024(i)

(b)(3):10 USC 424,(b)(3):50 USC 3024(i)

(b)(3):10 USC 424,(b)(3):50 USC 3024(i)

(b)(3):10 USC 424,(b)(3):50 USC 3024(i)

(b)(3):10 USC 424,(b)(3):50 USC 3024(i)